SIAM J. Applied Dynamical Systems
Vol. 13, No. 4, pp. 1353–1386

Decomposition of Nonlinear Delayed Networks around Cluster States with Applications to Neurodynamics*

Gábor Orosz†

Abstract. The dynamics of networked systems with delayed coupling are analyzed in this paper. Two theorems are stated which give conditions for decomposability of the dynamics in the vicinity of cluster states based on the intracluster and intercluster connectivity. Moreover, a decomposition method is presented that allows the derivation of delayed modal equations about cluster states even when heterogeneity is introduced into the linearized system due the nonlinearities in the coupling. Analytical tools are applied to these modal equations to derive exact stability conditions: the D-subdivision method is used to study the stability of equilibria, while the stability of periodic orbits is investigated using Floquet theory. The coexistence of multiple stable and unstable steady and oscillatory cluster states is investigated in a system of type II neurons where weakly and strongly asymmetric cluster oscillations are discovered.

Key words. time delay, clustering dynamics, decomposition, stability, Hopf bifurcations, Floquet theory, neural oscillations

AMS subject classifications. 34K18, 34K19, 37F99, 37N25, 92B25

DOI. 10.1137/130915637

1. Introduction.

One of the important scientific challenges of the 21st century is understanding natural and man-made complex systems. Examples include neural networks, gene regulatory networks in biology, and communication networks and multivehicle systems in the technological world. The behavior of such systems cannot be determined by simply looking at the individual elements (neurons, genes, servers, cars), but the system behavior emerges through the interactions between these elements. One of the major challenges is building parsimonious mathematical models that can adequately describe the dynamics of these complex systems and predict the time evolution of the patterns of activity. Such models must capture the dynamics of the elements, the interconnection structure, and the information transmission between the elements, while the model must remain scalable for large systems.

For example, in neural systems the dynamics of a single neuron (the time evolution of the membrane potential and the ion transport at the soma) can be represented by a particular neuromodel (Hodgkin–Huxley, Morris–Lecar, FitzHugh–Nagumo [16, 23, 39]), that is, by a set of ordinary differential equations (ODEs), while the connectivity of neurons can be described using directed graphs [35]. However, to describe signal propagation along the axons in detail, one needs to use partial differential equations (PDEs), and additional ODEs may be required to describe the chemical processes at synapses [16]. Such a modeling framework is only feasible for a relatively small number of neurons. To avoid this problem, signal transmission is often

*Received by the editors April 4, 2013; accepted for publication (in revised form) by J. Sieber July 5, 2014; published electronically October 9, 2014.
http://www.siam.org/journals/siads/13-4/91563.html
†Department of Mechanical Engineering, University of Michigan, Ann Arbor, MI 48109 (orosz@umich.edu).

considered instantaneous, which significantly reduces the predictive power of the model. In this paper, we consider a modeling framework where signal transmission is not modeled in detail, but the time it takes to transmit the signal is accounted for using time delays. This approach results in delay differential equations (DDEs), which retain the essential infinite dimensionality of the original dynamics, while the models remain scalable for large networks [4, 9, 48]. This modeling scenario can be used for a wide range of applications. For example, in genetic networks, delays represent the time needed for DNA transcription and protein folding [42, 52], while delays also appear in the immune response when an organism is fighting pathogens or viruses [3, 32, 55]. In vehicular systems the delay accounts for driver reaction time [24, 44], and it also appears in digital communications networks due to buffering [26].

Despite the parsimoniousness of the models, the resulting large systems of nonlinear DDEs require novel mathematical approaches that allow one to extract the skeleton of the dynamics. Clearly, a large number of stable and unstable spatiotemporal patterns may coexist in a large nonlinear system, including equilibria, periodic and quasi-periodic oscillations, and even chaotic motion. It is a difficult task to map these solutions out using straightforward numerical simulations without having prior knowledge of where they lie in state space.

In the control literature, the defining works [37, 38] on the decomposition of linear time-invariant networked systems gave rise to a number of extensions that can deal with higher dimensional node dynamics and can formally analyze the linear stability of the consensus state (synchronized equilibrium) in the presence of delay [6, 28, 30, 31]. Similar decomposition methods, called the master stability approaches [45], were developed in the physics literature where nonlinear node dynamics with linear coupling were considered with applications ranging from laser networks to neural networks [11, 17, 27]. When these systems are linearized about the synchronized equilibrium, the equations become analogous to those in consensus problems. Considering special oscillators (e.g., Stuart–Landau oscillators) and linear coupling, one may still obtain equations with time-independent coefficients when linearizing about periodic orbits [7]. Finally, we remark that in the physics literature, stability is usually determined numerically by calculating Lyapunov exponents independently of whether they focus on equilibria, oscillations, or even chaos [25]. This may be difficult to use when multiple stable and unstable states of different kinds coexist.

While synchronous states are important in many applications, there exists experimental evidence that neural systems use cluster states to process environmental information and perform neurocomputation [22, 40]. In such states, neurons within a chosen cluster exhibit the same temporal behavior, while each cluster exhibits different behavior. (Indeed, the synchronous state can be viewed as a special cluster state.) The existence of different cluster configurations was linked to symmetries in the network structure (described by symmetry groups) in [1, 12, 13, 46]. This concept was extended to delayed networks with linear diffusive coupling in [51], where sufficient conditions were provided for the stability of clustering manifolds using Lyapunov functionals. Symmetries were also identified and the intracluster dynamics were eliminated in "unidirectional" networks in [2], while in [14] the intracluster dynamics were analyzed in detail for partitioned networks. These methods allow one to identify the admissible cluster states in complex systems, but they fail to provide information on whether the dynamics can be decomposed in the vicinity of cluster states and how such decomposition should be attempted. Such decomposition tools are necessary if one wishes to

investigate cluster states in systems of realistic size, and this paper focuses on this challenging problem.

We apply rigorous mathematical techniques from dynamical systems theory to analyze the clustering dynamics of nonlinear oscillators connected via nonlinear delayed coupling. First, we show that one can identify all realizable cluster configurations by using simple set partitioning algorithms and the coupling matrix of the system. Then, we state *theorems of decomposability around cluster states*, which may contain clusters of different sizes, by extending the notions of *tangential stability* and *transversal stability* [41] to delayed networks. Our theorems, for the first time, give conditions for the intracluster and intercluster connectivity that allows decomposition of network dynamics in the vicinity of cluster states. Indeed, the existence of a cluster state does not imply decomposability of the dynamics. We also provide tools for decomposition that can be applied even when nonlinear coupling introduces heterogeneities into the corresponding linearized system while considering nonequally sized clusters. We remark that the decomposition can be performed for networks consisting of large numbers of elements since no detailed knowledge is required about the symmetries in the system.

By applying such decomposition tools, we provide *necessary and sufficient conditions for the linear stability of equilibria and periodic orbits* (as opposed to sufficient conditions for the stability of clustering manifolds [51] or numerical simulation-based results [25]). The D-subdivision method and Stépán's formulae [50] are used to derive the analytical stability charts for the time-invariant delayed modal equations describing the motion about cluster equilibria. On the other hand, we utilize Floquet theory [19] to analyze the delayed modal equations with time-varying coefficients that describe the dynamics in the vicinity of cluster oscillations. We remark that our analysis is not restricted to phase-locked solutions but allows the investigation of asymmetric cluster oscillations where both the number of oscillators and the shape of the oscillation profile can be different in each cluster; this has not been addressed before. To calculate the spectrum of the arising monodromy operators (i.e., Floquet multipliers) we utilize numerical continuation [47]. Alternatively, one may also use semi-discretization to calculate the multipliers [19].

To demonstrate the power of the mathematical approach, we apply our results to a neurosystem where the delay represents the signal propagation time along the axons. Analyzing periodic orbits that represent different clustering behavior is particularly relevant for this example because neural systems consist of nonlinear elements and use various rhythmic patterns to perform computation and encode information [34, 22, 54]. In the seminal work [8], the oscillations of piecewise smooth neuromodels were investigated with gap junction (without delay), and the Floquet multipliers were calculated analytically for the synchronized state. We adopt a smoothed version of the type II model derived in [8], extend it by adding signal transmission delays, and analyze the corresponding cluster states (both equilibria and oscillations). We show that where the phase oscillator approach [5, 15, 21, 36, 41] only predicts phase-locked solutions, our method reveals weakly and strongly asymmetric cluster oscillations.

The remainder of the paper proceeds as follows. After presenting the general modeling framework in section 2, we state a theorem for decomposability based on the network structure and provide mathematical tools for decomposition in section 2.1. These theoretical results are illustrated in section 2.2 through an example. In section 2.3 we state a theorem for semidecomposability by relaxing some conditions required for decomposability. The tools

used for stability analysis are explained in section 2.4, while the special case of all-to-all coupling is presented in section 2.5. The theoretical results are applied to a neural system in section 3: synchronous dynamics is discussed in section 3.1 followed by the analysis of two-cluster states in section 3.2. Finally, we conclude our results and state future research directions in section 4.

2. Decomposition of networks about cluster states. In this paper, a system consisting of N identical nonlinear oscillators coupled with identical nonlinear couplings is considered in the form

$$\dot{x}_i(t) = f\big(x_i(t)\big) + \frac{1}{N}\sum_{j=1}^{N} a_{ij}\, g\big(x_i(t), x_j(t-\tau)\big) \tag{2.1}$$

for $i = 1, \ldots, N$, where the dot represents differentiation with respect to time t. The internal state of oscillator i is captured by the vector $x_i \in \mathbb{R}^n$, and the internal dynamics consist of a set of nonlinear ODEs $\dot{x}_i = f(x_i)$. The coupling terms are described by the nonlinear function $g(x_i, x_j)$ that depends on the states of the interacting nodes. The time delay τ is the time needed for the "unmodeled" signal transmission processes to take place (e.g., to transmit signals along the axons in neural systems). The coupling structure of the system is captured by a directed graph, whose elements are represented by the coefficients of the N-dimensional interconnection/adjacency matrix defined as

$$a_{ij} = \begin{cases} 1 & \text{if node } j \text{ is connected to node } i, \\ 0 & \text{otherwise,} \end{cases} \tag{2.2}$$

$i, j = 1, \ldots, N$. We will use the abbreviated notation $A_N = [a_{ij}]$. Referring to the graph representation of the network, the oscillators are often called nodes, and the connections between them are called edges. For weighted graphs, definition (2.2) may be generalized by allowing a_{ij} to be a real number representing the coupling strength between two nodes. In this paper we assume that A_N is diagonalizable; that is, if an eigenvalue has algebraic multiplicity m, then it also has geometric multiplicity m, resulting in m linearly independent eigenvectors. Our decomposition method is still applicable when this condition does not hold, but the algebraic calculations become more involved. In addition, one may consider external inputs, which are omitted here for simplicity.

System (2.1) may admit a variety of different cluster solutions. Let us consider the K-cluster configuration where the clusters contains $[\, b_1 \quad b_2 \quad \cdots \quad b_K \,]$ oscillators, such that $\sum_{k=1}^{K} b_k = N$. Note that each b_k can be different. Indeed, $1 \le K \le N$, where $K = 1$ corresponds to full synchrony, while for $K = N$ no oscillators are grouped together; see also [41]. To simplify the notation we introduce

$$B_\ell = \sum_{k=1}^{\ell} b_k\,. \tag{2.3}$$

Indeed, $B_1 = b_1$, $B_K = N$, and, by definition, $B_0 = 0$. Thus, a *K-cluster state* can be defined as

$$x_i(t) = x_{c\ell}(t), \quad i = B_{\ell-1} + 1, \ldots, B_\ell, \quad \ell = 1, \ldots, K, \tag{2.4}$$

for all t. In state space this corresponds to an invariant manifold that we call the *clustering manifold*. By substituting (2.4) into (2.1) one obtains the DDEs

$$\dot{x}_{c\ell}(t) = f\big(x_{c\ell}(t)\big) + \frac{1}{N}\sum_{k=1}^{K} m_{\ell k}\, g\big(x_{c\ell}(t), x_{ck}(t-\tau)\big) \tag{2.5}$$

for $\ell = 1, \ldots, K$. Here the subrow sum

$$m_{\ell k} = \sum_{j=B_{k-1}+1}^{B_k} a_{ij} \tag{2.6}$$

must be the same for all $i = B_{\ell-1}+1, \ldots, B_\ell$ to ensure the existence of the K-cluster state. In fact, the K-dimensional matrix $M_K = [m_{\ell k}]$ can be viewed as a weighted adjacency matrix for the tangential dynamics [2].

To find the cluster configurations that can be realized by the system (2.1), the constant subrow sum condition (2.6) has to be checked for all admissible cluster configurations. These can be identified by partitioning a set of N distinguishable elements into K indistinguishable nonempty sets. The number of K-cluster configurations is given by the Stirling number of the second kind

$$S(N,K) = \frac{1}{K!}\sum_{\ell=0}^{K-1}(-1)^{\ell}\binom{K}{\ell}(K-\ell)^N, \tag{2.7}$$

while the total number of clusters is given by the Bell number

$$B(N) = \sum_{K=0}^{N} S(N,K). \tag{2.8}$$

In Appendix A all possible cluster configurations are determined for two different networks of seven oscillators by using a simple set partitioning algorithm [29] and (2.6). These examples will be used in sections 2.2 and 2.3 to demonstrate our decomposition method.

We remark that one may try to identify the realizable cluster configurations by studying the action of permutation matrices on the adjacency matrix (2.2). In particular, if there exists an N-dimensional permutation matrix P_N, such that $P_N A_N P_N^{-1} = A_N$, then there exists a corresponding invariant manifold in state space; see the examples in [51]. However, the reverse may not hold; that is, the existence of a clustering manifold may not imply the invariance of the adjacency matrix under permutation. This is demonstrated by the examples in Appendix A. The same two-cluster configuration can be realized by both systems, but in the second case no permutation matrix leaves the adjacency matrix invariant. Without such a property it is difficult to identify the symmetry since it requires one to show the existence of solution for a matrix equation; see Lemma 3 in [51]. Below we present a decomposition method that relies on the cluster configurations but does not require detailed knowledge of symmetries. We emphasize again that the existence of a clustering manifold does not guarantee decomposability of dynamics around the cluster states embedded in the manifold. Finally,

we remark that both (2.1) and (2.4) require infinite dimensional state spaces, and the initial conditions are functions on the time interval $[-\tau, 0]$. This means that the clustering manifold (2.4) is infinite dimensional.

Notice that definition (2.4) allows cluster states to be equilibria, periodic orbits, and even more complicated orbits. The only restriction is that the motion must remain in the corresponding (infinite dimensional) subspace. For example, cluster equilibria can be defined as

$$x_{c\ell}(t) \equiv x^*_{c\ell}, \quad \ell = 1, \dots, K, \tag{2.9}$$

and can be derived from the algebraic equations

$$0 = f\big(x^*_{c\ell}\big) + \frac{1}{N} \sum_{k=1}^{K} m_{\ell k}\, g\big(x^*_{c\ell}, x^*_{ck}\big); \tag{2.10}$$

cf. (2.5). Indeed, the solution may not be unique, and, even if it is unique, there may exist multiple K-cluster configurations that can be obtained via the permutation of oscillations. Notice that the delay does not influence the existence of these states but can influence their stability, as explained below.

Oscillatory cluster states can be defined as

$$x_{c\ell}(t) = x^{\mathrm{p}}_{c\ell}(t) = x^{\mathrm{p}}_{c\ell}(t + T_{\mathrm{p}}), \quad \ell = 1, \dots, K, \tag{2.11}$$

for all t, where T_{p} denotes the period of oscillations. These states can be obtained by solving the boundary value problem (2.5), (2.11) with periodic boundary conditions. Here the delay influences the shape as well as the stability of these orbits. Similar to equilibria, there may exist multiple solutions for a given parameter set. Notice that (2.11) incorporates phase-locked solutions where the oscillation profiles of the individual clusters differ only in phase. However, apart from this special case, our definition also incorporates cases where this spatiotemporal symmetry is broken and oscillation profiles are different for each cluster. Moreover, (2.5) also allows "mixed" cluster states where some clusters are in equilibrium while others are oscillating. In section 3 we will show examples of such symmetry breaking and mixed cluster states. Finally, we remark that more complicated motion (e.g., quasi-periodic and chaotic) may also appear for certain parameter sets, but these are not analyzed in this paper.

In order to linearize the system around the K-cluster state (2.4), we define the perturbations

$$y_i = x_i - x_{c\ell}, \quad i = B_{\ell-1} + 1, \dots, B_\ell, \quad \ell = 1, \dots, K, \tag{2.12}$$

so the Taylor expansion of (2.1) yields

$$\dot{y}_i(t) = L_\ell\, y_i(t) + \sum_{k=1}^{K} R_{\ell k} \left(\sum_{j=B_{k-1}+1}^{B_k} a_{ij}\, y_j(t - \tau) \right) \tag{2.13}$$

for $i = 1, \dots, N$. When linearizing about cluster equilibria (2.9) the $n \times n$ matrices $L_\ell, R_{\ell k}$ are time-independent, that is,

$$
\begin{aligned}
L_\ell^* &= Df\big(x_{c\ell}^*\big) + \frac{1}{N} \sum_{k=1}^{K} m_{\ell k}\, D^{(1)} g\big(x_{c\ell}^*, x_{ck}^*\big)\,, \\
R_{\ell k}^* &= \frac{1}{N}\, D^{(2)} g\big(x_{c\ell}^*, x_{ck}^*\big),
\end{aligned}
\tag{2.14}
$$

where and $D^{(1)}$ and $D^{(2)}$ represent derivatives with respect to the first and second variables, respectively. This means that (2.13) is a linear time-invariant system allowing the use of analytical techniques like the D-subdivision method and Stépán's formulae [50]. However, when linearizing about oscillatory cluster states (2.11), the matrices become time-periodic with period T_{p}, i.e.,

$$
\begin{aligned}
L_\ell^{\mathrm{p}}(t) &= Df\big(x_{c\ell}^{\mathrm{p}}(t)\big) + \frac{1}{N} \sum_{k=1}^{K} m_{\ell k}\, D^{(1)} g\big(x_{c\ell}^{\mathrm{p}}(t), x_{ck}^{\mathrm{p}}(t-\tau)\big) = L_\ell^{\mathrm{p}}(t+T_{\mathrm{p}})\,, \\
R_{\ell k}^{\mathrm{p}}(t) &= \frac{1}{N}\, D^{(2)} g\big(x_{c\ell}^{\mathrm{p}}(t), x_{ck}^{\mathrm{p}}(t-\tau)\big) = R_{\ell k}^{\mathrm{p}}(t+T_{\mathrm{p}})\,.
\end{aligned}
\tag{2.15}
$$

To analyze these equations one must use Floquet theory. As the corresponding monodromy operators usually cannot be written in closed form, numerical techniques like full discretization [47] or semi-discretization [19] must be deployed.

Defining $\mathbf{y} = \mathrm{col}\,[\,y_1 \;\; y_2 \;\; \dots \;\; y_N\,] \in \mathbb{R}^{nN}$, the linear system (2.13) can be rewritten as

$$
\dot{\mathbf{y}}(t) = (I_N \otimes L_\ell)\, \mathbf{y}(t) + (A_N \otimes R_{\ell k})\, \mathbf{y}(t-\tau)\,,
\tag{2.16}
$$

where I_N is the N-dimensional unit matrix, A_N is the adjacency matrix given in (2.2), and the subscripts ℓ and k are kept to emphasize that the blocks depend on which cluster is considered; see the example (2.27). For linear node dynamics (with identical nodes), L_ℓ would be independent of ℓ. Similarly, if the coupling were linear [7, 51], then $R_{\ell k}$ would be independent of ℓ and k, while nonlinear coupling introduces heterogeneity into the linearized system. Finally, we emphasize that we consider the general case of nonequally sized clusters.

2.1. Two-step decomposition. Instead of analyzing the stability of system (2.16) directly, we apply a two-step decomposition method. Our goal is to block diagonalize the matrix $A_N \otimes R_{\ell k}$ while keeping $I_N \otimes L_\ell$ block diagonal. The first step is based on the generalization of the concepts of *tangential stability* and *transversal stability* for delay networks that has been established for phase oscillators in [41]. This relies on the observation that a cluster state may lose stability in two qualitatively different ways. *Tangential stability loss* occurs when the cluster state loses stability so that the cluster configuration is kept. Such behavior occurs within the clustering manifold (2.4) and is characterized by the linearization of (2.5). On the other hand, *transversal stability loss* corresponds to splitting at least one cluster, which drives the system away from the clustering manifold. We remark that similar ideas can be used when analyzing the synchronized equilibrium of networks with hierarchical structures [10, 20, 49].

First, we separate the tangential dynamics and the transversal dynamics so that the transversal dynamics of individual clusters are also separated from each other. The following

theorem gives the condition of separability based on the adjacency matrix (2.2) that describes the network structure.

Theorem 1 (decomposability). *Assume that the intracluster connectivity within each cluster is represented by a regular graph; that is, the subrow and the subcolumn sums satisfy*

$$m_{\ell\ell} = \sum_{j=B_{\ell-1}+1}^{B_\ell} a_{ij} = \sum_{i=B_{\ell-1}+1}^{B_\ell} a_{ij} \tag{2.17}$$

for all admissible $i, j = B_{\ell-1}+1, \dots, B_\ell$, $\ell = 1, \dots, K$. *Moreover, assume that the intercluster connectivity is either complete or missing; that is,*

$$a_{ij} = 1 \quad or \quad 0 \quad \Rightarrow \quad m_{\ell k} = b_k \quad or \quad 0 \tag{2.18}$$

for all $i = B_{\ell-1}+1, \dots, B_\ell$ *and* $j = B_{k-1}+1, \dots, B_k$ *when* $\ell \neq k$, $\ell, k = 1, \dots, K$. *Then there exists a coordinate transformation that separates the tangential and transversal subspaces.*

We propose the coordinate transformation

$$\mathbf{y} = (T_N^K \otimes I)\, \mathbf{z}\,, \tag{2.19}$$

where the N-dimensional matrix T_N^K can be chosen so that the first K column vectors are defined by

$$\left(T_N^K\right)_{ij} = \begin{cases} 1 & \text{if} \quad i = B_{\ell-1}+1, \dots, B_\ell \quad \text{and} \quad j = \ell\,, \\ 0 & \text{otherwise} \end{cases} \tag{2.20}$$

for $\ell = 1, \dots, K$, and the remaining $N - K$ column vectors are defined as

$$\left(T_N^K\right)_{ij} = \begin{cases} 1 & \text{if} \quad i = B_{\ell-1}+1 \quad \text{and} \quad j = K + B_{\ell-1} - (\ell-1) + p\,, \\ -1 & \text{if} \quad i = B_{\ell-1}+1+p \quad \text{and} \quad j = K + B_{\ell-1} - (\ell-1) + p\,, \\ 0 & \text{otherwise} \end{cases} \tag{2.21}$$

for $p = 1, \dots, b_\ell - 1$, $\ell = 1, \dots, K$; see (2.28), where $N = 7$, $K = 2$, $[\,b_1 \;\; b_2\,] = [\,3 \;\; 4\,]$.

The detailed proof of Theorem 1 is given in Appendix B. The key idea behind (2.19), (2.20), (2.21) is that (2.20) spans the subspace corresponding to tangential dynamics, while for each ℓ (2.21) spans the subspace corresponding to transversal dynamics of that particular cluster. Note that this transformation does not require the calculation of the eigenvectors of A_N (that may be challenging for large systems) and that the decomposed system consists of equations that have clear physical meaning in terms of the clustering dynamics. The tangential dynamics correspond to motions that keep the cluster configuration intact. For example, equilibria may lose stability and create periodic oscillations without breaking the clusters. Further bifurcations may lead to more complicated (e.g., quasi-periodic or even chaotic) motions that are still contained by the clustering manifold. On the other hand, the transversal dynamics for each cluster describe the ways the cluster can be split, leading the system away from the clustering manifold (toward cluster states embedded in "higher-dimensional" manifolds).

We remark that if the intercluster connectivity is complete between all clusters (i.e., all a_{ij}'s are 1's in (2.18)), then the whole system is described by a regular graph; that is, all row sums and column sums of the adjacency matrix (2.2) are equal. This also holds if the connectivity is missing everywhere (i.e., all a_{ij}'s are 0's in (2.18)). These are the only ways to obtain regular graphs (except if one considers the special case of equally sized clusters). However, in general, regularity does not imply decomposability: for regular graphs the transformation (2.19), (2.20), (2.21) separates the tangential dynamics from the transversal dynamics but does not separate the transversal dynamics of individual clusters from each other.

Applying (2.19), (2.20), (2.21) to (2.16), the first K tangential equations take the form

$$\dot{z}_\ell(t) = L_\ell z_\ell(t) + \sum_{k=1}^{K} m_{\ell k}\, R_{\ell k}\, z_k(t-\tau) \tag{2.22}$$

for $\ell = 1, \dots, K$, which is indeed the linearization of (2.5). The corresponding eigenvalues Λ_ℓ, $\ell = 1, \dots, K$, of A_N are called tangential eigenvalues as these correspond to eigendirections that keep the K-cluster formation. However, these eigenvalues do not appear explicitly in (2.22), and this system is typically not block diagonalizable: even if one is able to find a transformation that block diagonalizes the delayed part, such a transformation usually makes the nondelayed part non–block diagonal.

In the remaining $N - K$ transversal equations each cluster ℓ is represented by $b_\ell - 1$ equations. In particular, defining $\hat{\mathbf{z}}_\ell = \mathrm{col}\,[\, z_{K+B_{\ell-1}-\ell+2} \quad \dots \quad z_{K+B_\ell-\ell}\,], \in \mathbb{R}^{n(b_\ell-1)}$, one may write these in the form

$$\dot{\hat{\mathbf{z}}}_\ell(t) = (I_{b_\ell-1} \otimes L_\ell)\, \hat{\mathbf{z}}_\ell(t) + (A_\ell \otimes R_{\ell\ell})\, \hat{\mathbf{z}}_\ell(t-\tau) \tag{2.23}$$

for $\ell = 1, \dots, K$, where A_ℓ is a $b_\ell - 1$-dimensional (weighted) cluster adjacency matrix. As the second decomposition step we block diagonalize (2.23) by using the transformation

$$\hat{\mathbf{z}}_\ell = (T_\ell \otimes I)\, \hat{\mathbf{q}}_\ell\,, \tag{2.24}$$

where $T_\ell = [\, f_{\ell,1} \quad \dots \quad f_{\ell,b_\ell-1}\,]$ so that $f_{\ell,i}$ is the ith eigenvector of the cluster adjacency matrix A_ℓ. Using this transformation, one may derive the modal equations

$$\dot{q}_i(t) = L_\ell\, q_i(t) + \Lambda_i\, R_{\ell\ell}\, q_i(t-\tau) \tag{2.25}$$

for $i = K + B_{\ell-1} - \ell + 2, \dots, K + B_\ell - \ell$, $\ell = 1, \dots K$, where Λ_i is the eigenvalue of A_ℓ. It can be shown that Λ_i are also the eigenvalues of A_N, and we refer to these as transversal eigenvalues as they correspond to splitting the K-cluster state.

2.2. Illustrative example. Let us illustrate the above two-step decomposition method using a simple example of a two-cluster state with cluster sizes $[\, b_1 \;\; b_2\,] = [\, 3 \;\; 4\,]$, i.e., $K = 2$, $N = b_1 + b_2 = 7$. Now let us consider a network with connectivity

$$A_7 = \left[\begin{array}{ccc:cccc} 0 & 0 & 1 & 1 & 1 & 1 & 1 \\ 1 & 0 & 0 & 1 & 1 & 1 & 1 \\ 0 & 1 & 0 & 1 & 1 & 1 & 1 \\ \hdashline 1 & 1 & 1 & 0 & 0 & 1 & 1 \\ 1 & 1 & 1 & 1 & 0 & 0 & 1 \\ 1 & 1 & 1 & 1 & 1 & 0 & 0 \\ 1 & 1 & 1 & 0 & 1 & 1 & 0 \end{array}\right], \tag{2.26}$$

which indeed allows the existence of two-cluster states with $b_1 = 3$ and $b_2 = 4$ as indicated by the constant subrow sums; cf. (2.6). (For completeness, all realizable cluster configurations are listed in Appendix A.) In this case (2.16) yields

(2.27)
$$\dot{\mathbf{y}}(t) = (I_7 \otimes L_\ell)\,\mathbf{y}(t) + (A_7 \otimes R_{\ell k})\,\mathbf{y}(t-\tau)$$
$$= \left[\begin{array}{ccc:c:ccc} L_1 & O & O & O & O & O & O \\ O & L_1 & O & O & O & O & O \\ O & O & L_1 & O & O & O & O \\ \hdashline O & O & O & L_2 & O & O & O \\ O & O & O & O & L_2 & O & O \\ O & O & O & O & O & L_2 & O \\ O & O & O & O & O & O & L_2 \end{array}\right] \mathbf{y}(t) + \left[\begin{array}{ccc:cccc} O & O & R_{11} & R_{12} & R_{12} & R_{12} & R_{12} \\ R_{11} & O & O & R_{12} & R_{12} & R_{12} & R_{12} \\ O & R_{11} & O & R_{12} & R_{12} & R_{12} & R_{12} \\ \hdashline R_{21} & R_{21} & R_{21} & O & O & R_{22} & R_{22} \\ R_{21} & R_{21} & R_{21} & R_{22} & O & O & R_{22} \\ R_{21} & R_{21} & R_{21} & R_{22} & R_{22} & O & O \\ R_{21} & R_{21} & R_{21} & O & R_{22} & R_{22} & O \end{array}\right] \mathbf{y}(t-\tau)\,,$$

where O is the n-dimensional matrix with zero elements.

The transformation matrix (2.20), (2.21) is constructed as

$$T_7^2 = \left[\begin{array}{cc:cc:ccc} 1 & 0 & 1 & 1 & 0 & 0 & 0 \\ 1 & 0 & -1 & 0 & 0 & 0 & 0 \\ 1 & 0 & 0 & -1 & 0 & 0 & 0 \\ \hdashline 0 & 1 & 0 & 0 & 1 & 1 & 1 \\ 0 & 1 & 0 & 0 & -1 & 0 & 0 \\ 0 & 1 & 0 & 0 & 0 & -1 & 0 \\ 0 & 1 & 0 & 0 & 0 & 0 & -1 \end{array}\right]. \tag{2.28}$$

Indeed, the first two columns correspond to keeping the two-cluster configuration (tangential directions), while the next two blocks span the subspaces corresponding to splitting the first or the second cluster, respectively (transversal directions). One can show that

$$(T_7^2 \otimes I)^{-1}(I_7 \otimes L_\ell)(T_7^2 \otimes I) = \left[\begin{array}{cc:cc:ccc} L_1 & O & O & O & O & O & O \\ O & L_2 & O & O & O & O & O \\ \hdashline O & O & L_1 & O & O & O & O \\ O & O & O & L_1 & O & O & O \\ \hdashline O & O & O & O & L_2 & O & O \\ O & O & O & O & O & L_2 & O \\ O & O & O & O & O & O & L_2 \end{array}\right]; \tag{2.29}$$

that is, only the order of the matrices in the diagonal changes. Moreover, one can also show that

(2.30)
$$(T_7^2 \otimes I)^{-1}(A_7 \otimes R_{\ell k})(T_7^2 \otimes I) = \left[\begin{array}{cc:cc:ccc} R_{11} & 4R_{12} & O & O & O & O & O \\ 3R_{21} & 2R_{22} & O & O & O & O & O \\ \hdashline O & O & -R_{11} & -R_{11} & O & O & O \\ O & O & R_{11} & O & O & O & O \\ \hdashline O & O & O & O & -R_{22} & -R_{22} & O \\ O & O & O & O & O & -R_{22} & -R_{22} \\ O & O & O & O & R_{22} & R_{22} & O \end{array}\right].$$

Thus, the tangential dynamics (2.22) are given by

$$\begin{bmatrix}\dot z_1(t)\\ \dot z_2(t)\end{bmatrix} = \begin{bmatrix}L_1 & O\\ O & L_2\end{bmatrix}\begin{bmatrix}z_1(t)\\ z_2(t)\end{bmatrix} + \begin{bmatrix}R_{11} & 4R_{12}\\ 3R_{21} & 2R_{22}\end{bmatrix}\begin{bmatrix}z_1(t-\tau)\\ z_2(t-\tau)\end{bmatrix}, \tag{2.31}$$

while the transversal equations in (2.23) are given by

$$\begin{bmatrix}\dot z_3(t)\\ \dot z_4(t)\end{bmatrix} = \begin{bmatrix}L_1 & O\\ O & L_1\end{bmatrix}\begin{bmatrix}z_3(t)\\ z_4(t)\end{bmatrix} + \begin{bmatrix}-R_{11} & -R_{11}\\ R_{11} & O\end{bmatrix}\begin{bmatrix}z_3(t-\tau)\\ z_4(t-\tau)\end{bmatrix} \tag{2.32}$$

and

$$\begin{bmatrix}\dot z_5(t)\\ \dot z_6(t)\\ \dot z_7(t)\end{bmatrix} = \begin{bmatrix}L_2 & O & O\\ O & L_2 & O\\ O & O & L_2\end{bmatrix}\begin{bmatrix}z_3(t)\\ z_4(t)\end{bmatrix} + \begin{bmatrix}-R_{22} & -R_{22} & O\\ O & -R_{22} & -R_{22}\\ R_{22} & R_{22} & O\end{bmatrix}\begin{bmatrix}z_5(t-\tau)\\ z_6(t-\tau)\\ z_7(t-\tau)\end{bmatrix}. \tag{2.33}$$

Using the eigenvectors of the cluster adjacency matrices

$$A_1 = \begin{bmatrix}-1 & -1\\ 1 & 0\end{bmatrix}, \quad A_2 = \begin{bmatrix}-1 & -1 & 0\\ 0 & -1 & -1\\ 1 & 1 & 0\end{bmatrix} \tag{2.34}$$

results in the transformations

$$T_1 = \begin{bmatrix}1 & 1\\ -\frac12 + \mathrm{i}\frac{\sqrt3}{2} & -\frac12 - \mathrm{i}\frac{\sqrt3}{2}\end{bmatrix}, \quad T_2 = \begin{bmatrix}1 & 1 & 1\\ -1 & \mathrm{i} & -\mathrm{i}\\ 1 & -1 & -1\end{bmatrix} \tag{2.35}$$

in (2.24), and thus, we obtain the block diagonal equations

$$\begin{bmatrix}\dot q_3(t)\\ \dot q_4(t)\end{bmatrix} = \begin{bmatrix}L_1 & O\\ O & L_1\end{bmatrix}\begin{bmatrix}q_3(t)\\ q_4(t)\end{bmatrix} + \begin{bmatrix}-\left(\frac12 + \mathrm{i}\frac{\sqrt3}{2}\right)R_{11} & O\\ O & -\left(\frac12 - \mathrm{i}\frac{\sqrt3}{2}\right)R_{11}\end{bmatrix}\begin{bmatrix}q_3(t-\tau)\\ q_4(t-\tau)\end{bmatrix} \tag{2.36}$$

and

$$\begin{bmatrix}\dot q_5(t)\\ \dot q_6(t)\\ \dot q_7(t)\end{bmatrix} = \begin{bmatrix}L_2 & O & O\\ O & L_2 & O\\ O & O & L_2\end{bmatrix}\begin{bmatrix}q_5(t)\\ q_6(t)\\ q_7(t)\end{bmatrix} + \begin{bmatrix}O & O & O\\ O & -(1+\mathrm{i})R_{22} & O\\ O & O & -(1-\mathrm{i})R_{22}\end{bmatrix}\begin{bmatrix}q_5(t-\tau)\\ q_6(t-\tau)\\ q_7(t-\tau)\end{bmatrix}; \tag{2.37}$$

cf. (2.25). Notice that some of the above equations contain complex coefficients. One may take the real and imaginary parts of these equations and obtain $2n$-dimensional systems with real coefficients [6, 39].

For completeness, we mention that one may change the intercluster coupling in (2.26) as shown by the matrices (B.12) in Appendix B that still satisfy Theorem 1. This only changes the tangential dynamics according to (B.13), while the transversal dynamics remain the same. Notice that matrix (2.26) also allows full synchrony as the row sums are constant, but none of matrices in (B.12) allow this state. Finally, we remark that even if the conditions of Theorem 1 are not satisfied, the transformation (2.19), (2.20), (2.21) still simplifies the system, as demonstrated in the next section.

2.3. Semidecomposability. Theorem 1 is quite restrictive regarding the connectivity structure of the system. In this section we relax some of these conditions and state a theorem that allows one to semidecompose the system, that is, to bring the corresponding matrices into an upper block triangular form.

First, to illustrate the idea, we modify example (2.26) shown in the previous section so that the conditions of Theorem 1 do not hold. In particular, we consider a network with connectivity

$$A_7 = \left[\begin{array}{ccc:c:ccc} 0&0&1&1&0&1&1\\ 1&0&0&1&1&0&1\\ 0&1&0&1&1&1&0\\ \hdashline 1&0&0&0&1&1&0\\ 1&0&0&1&0&1&0\\ 1&0&0&1&0&0&1\\ 1&0&0&1&1&0&0 \end{array}\right]. \tag{2.38}$$

This, similarly to (2.26), allows the existence of a two-cluster state with cluster sizes $[\,b_1\ \ b_2\,] = [\,3\ \ 4\,]$, as indicated by the corresponding constant subrow sums; cf. (2.6). (For completeness, all realizable cluster configurations are listed in Appendix A.)

In this case, using (2.28), we obtain

$$(T_7^2 \otimes I)^{-1}(A_7 \otimes R_{\ell k})(T_7^2 \otimes I) = \left[\begin{array}{cc:cc:ccc} R_{11} & 3R_{12} & O & O & \frac{1}{3}R_{12} & \frac{1}{3}R_{12} & \frac{1}{3}R_{12}\\ R_{21} & 2R_{22} & R_{21} & R_{21} & \frac{1}{4}R_{22} & \frac{1}{4}R_{22} & \frac{1}{2}R_{22}\\ \hdashline O & O & -R_{11} & -R_{11} & \frac{1}{3}R_{12} & -\frac{2}{3}R_{12} & \frac{1}{3}R_{12}\\ O & O & R_{11} & O & \frac{1}{3}R_{12} & \frac{1}{3}R_{12} & -\frac{2}{3}R_{12}\\ \hdashline O & O & O & O & -\frac{3}{4}R_{22} & \frac{1}{4}R_{22} & -\frac{1}{2}R_{22}\\ O & O & O & O & -\frac{3}{4}R_{22} & -\frac{3}{4}R_{22} & \frac{1}{2}R_{22}\\ O & O & O & O & \frac{1}{4}R_{22} & -\frac{3}{4}R_{22} & -\frac{1}{2}R_{22} \end{array}\right]. \tag{2.39}$$

The blocks outside the "diagonal" correspond to how (2.38) violates Theorem 1. The 4×4 block at the bottom right of (2.38) is not regular as the subcolumn sums are not constant. Consequently, the orthogonality condition (B.7) does not hold, which results in the terms R_{22} in the upper triangle in (2.39). Similarly, the 4×3 block at the bottom left of (2.38) is neither full of zeros nor full of ones. In particular, having nonconstant subcolumn sums leads to the violation of the orthogonality condition (B.11). Consequently, the terms R_{21} appear in the upper triangle. Notice that (B.10) still holds for this block since each column is either full of zeros or full of ones. Finally, the 3×4 block at the top right of (2.38) violates both orthogonality conditions (B.10), (B.11) and leads to the terms R_{12} in the upper triangle.

We remark that violating (B.7) or (B.10) always results in terms in the upper triangle. On the other hand, violating (B.11) in a block in the lower triangle of (2.38) results in terms in the upper as well as in the lower triangles of (2.39). Still, by rearranging the order of clusters one may "transfer" everything to the upper triangle. In general, such rearrangement is only possible if there are no loops in the aggregated graphs consisting of intercluster connections that violate (B.11). Based on these arguments we can state the following theorem.

Theorem 2 (semidecomposability). *Assume that the subrow sum* (2.6) *is constant and the intercluster connections that violate* (B.11) *do not form loops; then the transformation* (2.19),

(2.20), (2.21) *and appropriate reordering of clusters result in an upper block triangular matrix in front of the delayed term.*

We remark that since the blocks at the diagonal have different sizes, (2.30) and (2.39) do not have the same eigenvalues, and, consequently, the elements in the upper triangle can influence stability.

2.4. Stability of cluster equilibria and cluster oscillations. In this section we present the analytical tools we use to derive necessary and sufficient conditions for the linear stability of cluster states. These allow us to derive a stability chart while focusing on a given type of cluster state (e.g., equilibrium or periodic orbit) as opposed to numerical tools based on Lyapunov exponents that only quantify the average attractivity in state space [25]. Lyapunov functionals may also be used to derive sufficient conditions of stability [51], but, with the neural applications in mind, we are interested in exact stability. The results below are explained for the fully decomposable systems presented in sections 2.1 and 2.2, but they can also be generalized for the semidecomposable systems discussed in section 2.3.

As mentioned above, when linearizing about cluster equilibria (2.9), the matrices $L_\ell, R_{\ell k}$ (2.14) are time-independent. Thus, in order to determine the stability of equilibria, the trial solutions $z_\ell(t) = Z_\ell\, \mathrm{e}^{\lambda t}$, $q_i(t) = Q_i\, \mathrm{e}^{\lambda t}$, $\lambda \in \mathbb{C}$, $Z_\ell, Q_i \in \mathbb{C}^n$ are substituted into (2.22), (2.25), which results in the characteristic equations

$$\det\left(\begin{bmatrix} \lambda I - L_1 & \cdots & O \\ \vdots & \ddots & \vdots \\ O & \cdots & \lambda I - L_K \end{bmatrix} - \frac{1}{N}\begin{bmatrix} m_{11}R_{11} & \cdots & m_{1K}R_{1K} \\ \vdots & \ddots & \vdots \\ m_{K1}R_{K1} & \cdots & m_{KK}R_{KK} \end{bmatrix} \mathrm{e}^{-\lambda\tau}\right) = 0 \tag{2.40}$$

and

$$\det(\lambda I - L_\ell - \Lambda_i R_{\ell\ell}\, \mathrm{e}^{-\lambda\tau}) = 0 \tag{2.41}$$

for $i = K + B_{\ell-1} - \ell + 2, \dots, K + B_\ell - \ell$, $\ell = 1, \dots, K$. The equilibrium is tangentially/transversally stable when all the infinitely many characteristic roots λ, given by (2.40)/(2.41), are located in the left-half complex plane. Indeed, the cluster equilibrium is linearly stable if both tangential and transversal stability are satisfied. Substituting $\lambda = \mathrm{i}\omega$, $\omega \geq 0$, into the above equations, one may obtain the tangential and transversal stability boundaries that divide the parameter space into stable and unstable domains. Stability can be evaluated by applying Stépán's formulae derived in [50]. The obtained stability boundaries also have clear physical meaning: crossing a tangential stability boundary from stable to unstable keeps the cluster configuration, while crossing a transversal boundary leads to cluster split. We remark that the oscillations arising from these instabilities may be studied analytically using normal form calculations in the vicinity of the stability boundaries [43]. As these calculations require approximation of nonlinearities, here we use numerical techniques to find the periodic orbits and evaluate their stability as explained below.

When linearizing about cluster oscillations (2.11), the matrices $L_\ell, R_{\ell k}$ (2.15) are time-periodic with period T_p. Instead of exponential trial solutions, one must use Floquet theory to determine stability; see [19]. This requires the reformulation of (2.22), (2.25) using the state variables $z_{\ell,t}(\theta) = z_\ell(t+\theta)$, $q_{i,t}(\theta) = q_i(t+\theta)$, $\theta \in [-\tau, 0]$, that are contained by the

infinite dimensional space of continuous functions. These states can be obtained from the initial functions as

$$\begin{bmatrix} z_{1,t} \\ \vdots \\ z_{K,t} \end{bmatrix} = \mathcal{U}_0(t) \begin{bmatrix} z_{1,0} \\ \vdots \\ z_{K,0} \end{bmatrix} \tag{2.42}$$

and

$$q_{i,t} = \mathcal{U}_i(t)\, q_{i,0} \tag{2.43}$$

for $i = K+1, \ldots, N$, where the solution operators $\mathcal{U}_0(t)$ and $\mathcal{U}_i(t)$ usually cannot be written in closed form. The eigenvalues of the monodromy operators $\mathcal{U}_0(T_\mathrm{p})$ and $\mathcal{U}_i(T_\mathrm{p})$ are called Floquet multipliers, and they determine the tangential and transversal stability of oscillations: if all these multipliers are smaller than 1 in magnitude, then the periodic solution is stable. Again (2.42) corresponds to tangential stability, while (2.43) corresponds to transversal stability, and crossing the corresponding stability boundaries in parameter space leads to qualitatively different behaviors.

To calculate the stability boundaries one needs to use numerical techniques. The first step is to compute the periodic orbit which is the solution of the boundary value problem (2.5), (2.11). This can be done by using numerical collocation, which can be merged with arc-length continuation to find the orbit when parameters are varied [47]. Since (2.22) is the linearization of (2.5), collocations provide a discretization of the monodromy operator $\mathcal{U}_0(T_\mathrm{p})$ in (2.42), and the corresponding eigenvalues (the tangential Floquet multipliers) can be computed numerically. Alternatively, semi-discretization can be used to compute the multipliers [19]. However, (2.25) also has to be evaluated at the periodic solution in order to compute the transversal Floquet multipliers which are the eigenvalues of $\mathcal{U}_i(T_\mathrm{p})$ in (2.43). To solve this problem we create augmented systems consisting of (2.5), (2.11), (2.25) which give the same periodic orbit as (2.5), (2.11) for the variables $x_{\mathrm{c}\ell}^\mathrm{p}$ while resulting in $q_i \equiv 0$. Each augmented system contains the tangential multipliers as well as transversal multipliers corresponding to the chosen cluster.

2.5. All-to-all coupled systems. In this section we consider all-to-all coupling without self-coupling. This admits the maximal number of cluster states and allows the derivation of general results without specifying the numbers of oscillators $[\, b_1 \;\; b_2 \;\; \cdots \;\; b_K \,]$ in each cluster or even the total number of oscillators N. Interaction between different cluster states can also be investigated as parameters are varied. The equations derived in this section will be applied in section 3 to study the cluster states of a neuromodel.

Let us consider the adjacency matrix

$$a_{ij} = \begin{cases} 1 & \text{if} \quad j \neq i, \\ 0 & \text{if} \quad j = i, \end{cases} \tag{2.44}$$

which implies

$$m_{\ell k} = \begin{cases} b_k - 1 & \text{if} \quad k = \ell, \\ b_k & \text{if} \quad k \neq \ell. \end{cases} \tag{2.45}$$

Moreover, the eigenvalues of the adjacency matrix are

$$\Lambda_1 = N-1, \quad \Lambda_i = -1, \quad i = 2, \dots, N, \tag{2.46}$$

and the corresponding eigenvectors are

$$e_1 = \begin{bmatrix} 1 \\ 1 \\ 1 \\ \vdots \\ 1 \end{bmatrix}, \; e_2 = \begin{bmatrix} 1 \\ -1 \\ 0 \\ \vdots \\ 0 \end{bmatrix}, \; e_3 = \begin{bmatrix} 1 \\ 0 \\ -1 \\ \vdots \\ 0 \end{bmatrix}, \dots, \; e_N = \begin{bmatrix} 1 \\ 0 \\ \vdots \\ 0 \\ -1 \end{bmatrix}. \tag{2.47}$$

The eigenvalue -1 has algebraic and geometric multiplicity $N-1$, and the eigenvectors $e_2, \dots, e_N$ span the corresponding subspace. Indeed, any linear combination of the eigenvectors also spans the subspace.

For the adjacency matrix (2.44) Theorem 1 holds for all possible cluster states. However, depending on which cluster state we focus on, the transformation matrix (2.19), (2.20), (2.21) must be chosen differently. For example, considering the fully synchronized state $x_i(t) = x_c(t)$, $i = 1, \dots, N$, with $K = 1$, $b_1 = N$, $m_{11} = N-1$, (2.5) simplifies to

$$\dot{x}_c(t) = f\big(x_c(t)\big) + \frac{N-1}{N}\, g\big(x_c(t), x_c(t-\tau)\big)\,. \tag{2.48}$$

When linearizing about the synchronous state, (2.13) yields

$$\dot{y}_i(t) = L\, y_i(t) + R \sum_{j=1, j\neq i}^{N} y_j(t-\tau) \tag{2.49}$$

for $i = 1, \dots, N$, where the index 1 of the matrices has been dropped for simplicity.

To separate the tangential and transversal dynamics we choose the transformation matrix

$$T_N^1 = \left[\begin{array}{c|cccc} 1 & 1 & 1 & \cdots & 1 \\ 1 & -1 & 0 & & 0 \\ \vdots & 0 & -1 & \ddots & \vdots \\ \vdots & \vdots & \vdots & \ddots & 0 \\ 1 & 0 & 0 & & -1 \end{array}\right], \tag{2.50}$$

which results in the modal equations

$$\begin{aligned} \dot{z}_1(t) &= L\, z_1(t) + (N-1) R\, z_1(t-\tau), \\ \dot{z}_i(t) &= L\, z_i(t) - R\, z_i(t-\tau), \qquad i = 2, \dots, N; \end{aligned} \tag{2.51}$$

cf. (2.22), (2.23), (2.25). The first equation (which is indeed the linearization of (2.48)) describes the tangential stability of the synchronized state, while the second equation describes transversal stability. Notice that the transversal part is already block diagonal; that is, no

further transformations are needed. This is because the corresponding columns of T_N^1 are in fact the eigenvectors of the adjacency matrix A_N.

For a general two-cluster state defined by $x_i(t) = x_{c1}(t)$, $i = 1, \dots, b_1$, and $x_i(t) = x_{c2}(t)$, $i = b_1 + 1, \dots, b_1 + b_2 = N$, we have $K = 2$ and

$$\begin{bmatrix} m_{11} & m_{12} \\ m_{21} & m_{22} \end{bmatrix} = \begin{bmatrix} b_1 - 1 & b_2 \\ b_1 & b_2 - 1 \end{bmatrix}; \tag{2.52}$$

cf. (2.45). That is, (2.5) gives

$$\begin{aligned} \dot{x}_{c1}(t) &= f\big(x_{c1}(t)\big) + \frac{b_1 - 1}{N} g\big(x_{c1}(t), x_{c1}(t-\tau)\big) + \frac{b_2}{N} g\big(x_{c1}(t), x_{c2}(t-\tau)\big), \\ \dot{x}_{c2}(t) &= f\big(x_{c2}(t)\big) + \frac{b_1}{N} g\big(x_{c2}(t), x_{c1}(t-\tau)\big) + \frac{b_2 - 1}{N} g\big(x_{c2}(t), x_{c2}(t-\tau)\big), \end{aligned} \tag{2.53}$$

while (2.13) yields

$$\begin{aligned} \dot{y}_i(t) &= L_1 y_i(t) + R_{11} \sum_{j=1, j\neq i}^{b_1} y_j(t-\tau) + R_{12} \sum_{j=b_1+1}^{N} y_j(t-\tau), \quad i = 1, \dots, b_1, \\ \dot{y}_i(t) &= L_2 y_i(t) + R_{21} \sum_{j=1}^{b_1} y_j(t-\tau) + R_{22} \sum_{j=b_1+1, j\neq i}^{N} y_j(t-\tau), \quad i = b_1 + 1, \dots, N. \end{aligned} \tag{2.54}$$

Indeed, tangential and transversal directions are defined differently for a two-cluster state than for the synchronous state. Here, to separate the tangential and transversal dynamics we use

$$T_N^2 = \left[\begin{array}{cc:ccccc:cccc} 1 & 0 & 1 & 1 & \cdots & 1 & 0 & 0 & \cdots & 0 \\ 1 & 0 & -1 & 0 & & 0 & 0 & 0 & \cdots & 0 \\ \vdots & \vdots & 0 & -1 & \ddots & \vdots & \vdots & \vdots & & \vdots \\ \vdots & \vdots & \vdots & \vdots & \ddots & 0 & \vdots & \vdots & & \vdots \\ 1 & 0 & 0 & 0 & & -1 & 0 & 0 & \cdots & 0 \\ \hdashline 0 & 1 & 0 & 0 & \cdots & 0 & 1 & 1 & \cdots & 1 \\ 0 & 1 & 0 & 0 & \cdots & 0 & -1 & 0 & & 0 \\ \vdots & \vdots & \vdots & \vdots & & \vdots & 0 & -1 & \ddots & \vdots \\ \vdots & \vdots & \vdots & \vdots & & \vdots & \vdots & \vdots & \ddots & 0 \\ 0 & 1 & 0 & 0 & \cdots & 0 & 0 & 0 & & -1 \end{array}\right], \tag{2.55}$$

which results in the modal equations

$$\begin{aligned} \begin{bmatrix} \dot{z}_1(t) \\ \dot{z}_2(t) \end{bmatrix} &= \begin{bmatrix} L_1 & O \\ O & L_2 \end{bmatrix} \begin{bmatrix} z_1(t) \\ z_2(t) \end{bmatrix} + \begin{bmatrix} (b_1 - 1)R_{11} & b_2 R_{12} \\ b_1 R_{21} & (b_2 - 1)R_{22} \end{bmatrix} \begin{bmatrix} z_1(t-\tau) \\ z_2(t-\tau) \end{bmatrix}, \\ \dot{z}_i(t) &= L_1 z_i(t) - R_{11} z_i(t-\tau), \qquad i = 3, \dots, b_1 + 1, \\ \dot{z}_i(t) &= L_2 z_i(t) - R_{22} z_i(t-\tau), \qquad i = b_1 + 2, \dots, N. \end{aligned} \tag{2.56}$$

The first equation (which is indeed the linearization of (2.53)) describes the tangential stability, while the second and third equations correspond to transversal stability of the first and the second clusters, respectively. Again, the transversal part is already block diagonal, as the transformation T_N^2 also uses the transversal eigenspace of the adjacency matrix A_N. Indeed, (2.55) and (2.56) can be generalized for any K, and the dynamics of the all-to-all coupled system can be understood by analyzing the different cluster configurations. To demonstrate the power of our approach we apply the techniques discussed above to a system of all-to-all coupled neurons in the next section.

3. Dynamics of type II neurons. Populations of neurons encode information and carry out computation by using spatiotemporal patterns of activity [34]. Stable and unstable cluster states and transitions between cluster states play an important role in this information processing [22, 40, 41]. In order to understand the underlying dynamics, the stability of cluster equilibria and cluster oscillations needs to be determined. Indeed, different cluster configurations may coexist for a chosen set of parameters, and multiple states may coexist in the corresponding subspaces. In this section we apply the methods described above to classify the admissible cluster states in a neurosystem and build up the dynamical elements of neurocomputation in a systematic way.

Mathematical models that describe the temporal dynamics of neurons are categorized as type I and type II neuromodels; see [8]. Type I neurons display arbitrarily low firing frequencies at firing threshold, which quickly increase as the magnitude of the applied current is increased. Type II neurons, on the other hand, exhibit a nonzero, "critical" firing frequency at threshold and have a much shallower slope in terms of the frequency changes as a function of the applied current. Here we consider a type II neuromodel, namely, a FitzHugh–Nagumo type model with direct electronic coupling (gap junctions):

$$\begin{aligned} C\dot{v}_i(t) &= h\big(v_i(t)\big) - w_i(t) + I + \frac{1}{N}\sum_{j=1}^{N} a_{ij}\,\kappa\cdot\big(v_j(t-\tau) - v_i(t)\big), \\ \dot{w}_i(t) &= v_i(t) - \gamma\, w_i(t), \end{aligned} \tag{3.1}$$

where

$$h(v_i) = v_i(1-v_i)(v_i-a). \tag{3.2}$$

We remark that while linear coupling is considered here for simplicity, all results can be generalized to nonlinear coupling as the decomposition method explained above is capable of handling the general case.

Each neuron is described by two scalar variables—the membrane potential at the soma v_i and a so-called gating variable w_i which represents the ion transport through the membrane. Comparing (3.1) with the general model (2.1), one can see that $x_i = \mathrm{col}\,[\,v_i \;\; w_i\,]$. The model also contains the following (scaled) parameters:

$$\begin{aligned} C &= 0.1 \quad \text{— membrane capacitance,} \\ I &= 0.5 \quad \text{— applied current,} \\ \gamma &= 0.5, \\ a &= 0.25. \end{aligned} \tag{3.3}$$

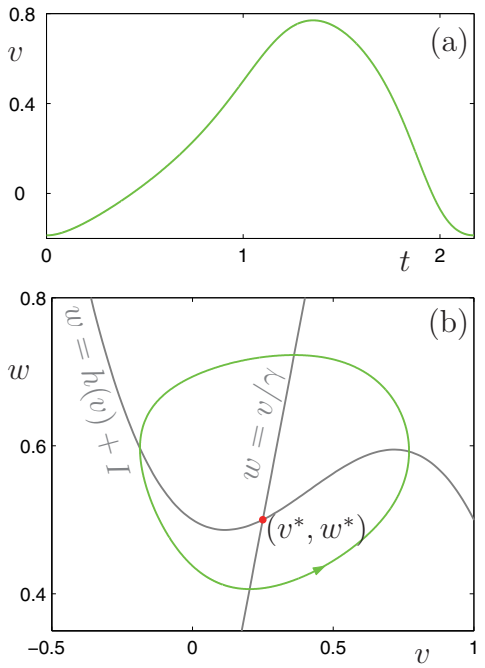

Figure 1. *Stable periodic solution of model* (3.1), (3.2) *for parameters* (3.3) *without coupling* $\kappa = 0$. *Panel* (a) *shows the variation of the voltage* v *as a function of time* t, *while panel* (b) *depicts the periodic orbit in state space where the equilibrium* $(v^*, w^*) = (0.25, 0.5)$ *is unstable.*

Without coupling, i.e., for $\kappa = 0$, equations (3.1), (3.2) with parameters (3.3) produce sustained oscillations of period $T_\mathrm{p} \approx 2.173$; see the stable periodic orbit in Figure 1. The coupling term $\kappa \cdot \big(v_j(t-\tau) - v_i(t)\big)$ represents a direct electronic connection between the axon of the jth neuron and the dendrites of the ith neuron. Here $v_i(t)$ is the postsynaptic potential, $v_j(t-\tau)$ is the presynaptic potential, κ is the conductance of the gap junction, and τ represents the signal propagation time along the axon of the jth neuron (dendritic delays are omitted here). That is, the presynaptic potential is equal to what the potential of the soma of the jth neuron was τ time before.

We consider a neurosystem with a high degree of connectivity, and, for simplicity, we assume all-to-all coupling without self-coupling, which was discussed in the previous section. This indeed allows all possible cluster configurations, but here we focus our attention on synchronous and two-cluster states (with nonequally sized clusters).

3.1. Synchrony of type II neurons. Consider the synchronous solutions $[\,v_i\ w_i\,] = [\,v_\mathrm{c}\ w_\mathrm{c}\,]$, $i = 1, \ldots, N$, for the neurosystem (3.1) with all-to-all coupling without self-coupling; cf. (2.44). In this case (2.48) results in the tangential dynamics

$$\begin{aligned} C\dot{v}_\mathrm{c}(t) &= h\big(v_\mathrm{c}(t)\big) - w_\mathrm{c}(t) + I + \frac{N-1}{N}\kappa \cdot \big(v_\mathrm{c}(t-\tau) - v_\mathrm{c}(t)\big), \\ \dot{w}_\mathrm{c}(t) &= v_\mathrm{c}(t) - \gamma\, w_\mathrm{c}(t). \end{aligned} \tag{3.4}$$

When linearizing the system about a synchronous state one obtains the matrices

$$L = \begin{bmatrix} \frac{1}{C}h'(v_c) - \frac{N-1}{N}\frac{\kappa}{C} & -\frac{1}{C} \\ 1 & -\gamma \end{bmatrix}, \quad R = \begin{bmatrix} \frac{1}{N}\frac{\kappa}{C} & 0 \\ 0 & 0 \end{bmatrix}, \tag{3.5}$$

which appear in (2.49) as well as in the decomposed system (2.51).

To obtain the synchronous equilibrium we substitute $[\,v_c(t) \;\; w_c(t)\,] \equiv [\,v_c^* \;\; w_c^*\,]$ into (3.4), which results in the algebraic equations

$$\begin{aligned} 0 &= h(v_c^*) - w_c^* + I, \\ 0 &= v_c^* - \gamma\, w_c^*. \end{aligned} \tag{3.6}$$

Notice that the coupling term disappears, and, consequently, the synchronized equilibrium is the same as the equilibrium of an uncoupled neuron (which may not be the case for more general nonlinear coupling). For parameters (3.3), we have a unique unstable equilibrium as shown by the red dot in Figure 1(b) at the intersection of the gray nullclines given by (3.6).

Using the notation $z_1 = [\,\tilde{v}_c \;\; \tilde{w}_c\,]$ and $z_i = [\,\tilde{v}_b \;\; \tilde{w}_b\,]$, $i = 2, \dots, N$, where the tilde represents perturbations and the subscripts c and b refer to synchronous and synchrony-breaking perturbations, the first equation in (2.51) yields

$$\begin{bmatrix} \dot{\tilde{v}}_c(t) \\ \dot{\tilde{w}}_c(t) \end{bmatrix} = \begin{bmatrix} -p-q & -\frac{1}{C} \\ 1 & -\gamma \end{bmatrix} \begin{bmatrix} \tilde{v}_c(t) \\ \tilde{w}_c(t) \end{bmatrix} + \begin{bmatrix} q & 0 \\ 0 & 0 \end{bmatrix} \begin{bmatrix} \tilde{v}_c(t-\tau) \\ \tilde{w}_c(t-\tau) \end{bmatrix}, \tag{3.7}$$

which is the linearization of (3.4), while the second equation in (2.51) results in

$$\begin{bmatrix} \dot{\tilde{v}}_b(t) \\ \dot{\tilde{w}}_b(t) \end{bmatrix} = \begin{bmatrix} -p-q & -\frac{1}{C} \\ 1 & -\gamma \end{bmatrix} \begin{bmatrix} \tilde{v}_b(t) \\ \tilde{w}_b(t) \end{bmatrix} + \begin{bmatrix} -r & 0 \\ 0 & 0 \end{bmatrix} \begin{bmatrix} \tilde{v}_b(t-\tau) \\ \tilde{w}_b(t-\tau) \end{bmatrix}, \tag{3.8}$$

where

$$\begin{aligned} p &= -\frac{1}{C}h'(v_c) = \frac{1}{C}\big(3(v_c)^2 - 2(a+1)v_c + a\big), \\ q &= \frac{N-1}{N}\frac{\kappa}{C}, \\ r &= \frac{1}{N}\frac{\kappa}{C}. \end{aligned} \tag{3.9}$$

In order to determine the tangential and transversal stability of the equilibrium, one must evaluate the matrices (3.5) at $[\,v_c^* \;\; w_c^*\,]$, which means that $p = -\frac{1}{C}h'(v_c^*)$ becomes a constant. The corresponding tangential and transversal characteristic equations become

$$\big(\lambda + p + q(1 - \mathrm{e}^{-\lambda\tau})\big)(\lambda + \gamma) + \frac{1}{C} = 0 \tag{3.10}$$

and

$$\big(\lambda + p + q + r\,\mathrm{e}^{-\lambda\tau})\big)(\lambda + \gamma) + \frac{1}{C} = 0; \tag{3.11}$$

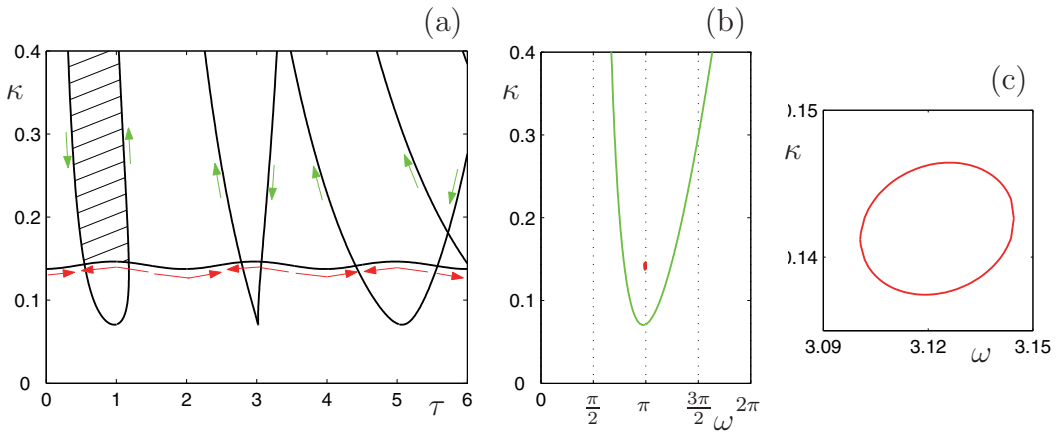

Figure 2. *Panel* (a) *depicts the stability chart representing changes in tangential stability (lobes) and transversal stability (horizontal curve) of the synchronized equilibrium. The green and red arrows show the variation of angular frequency* ω *along the curves. This change is also represented in panel* (b)*, and a zoom is shown in panel* (c)*. In the dashed domain in panel* (a) *the synchronized equilibrium is both tangentially and transversally stable.*

cf. (2.40) and (2.41). To find the stability boundaries we substitute $\lambda = \mathrm{i}\omega$ into (3.10) and (3.11), separate the real and imaginary parts, and, after some algebraic manipulation, we obtain the boundaries for tangential stability,

$$\begin{aligned} \tau &= \frac{2}{\omega}\left(\arctan\left[\frac{\beta}{\alpha}\right] + \ell\pi\right), \quad \ell = 0, 1, 2, \dots, \\ \kappa &= -\frac{CN}{2(N-1)}\frac{\delta}{\beta}, \end{aligned} \tag{3.12}$$

and for transversal stability,

$$\begin{aligned} \tau &= \frac{2}{\omega}\left(\arctan\left[\frac{-\beta/\alpha \pm \sqrt{\beta^2/\alpha^2 - (N-2)}}{N-2}\right] + \ell\pi\right), \quad \ell = 0, 1, 2, \dots, \\ \kappa &= \frac{C}{N-2}\left(-(N-1)\beta \pm \sqrt{(N-1)^2\beta^2 - (N-2)\delta}\right), \end{aligned} \tag{3.13}$$

where

$$\begin{aligned} \alpha &= \omega - \frac{1}{C}\frac{\omega}{\gamma^2+\omega^2}, \\ \beta &= p + \frac{1}{C}\frac{\gamma}{\gamma^2+\omega^2}, \\ \delta &= p^2 + \omega^2 + \frac{1}{C}\frac{1}{\gamma^2+\omega^2}\left(\frac{1}{C} + 2p\gamma - 2\omega^2\right). \end{aligned} \tag{3.14}$$

The corresponding curves are plotted for $N = 33$ in the (τ, κ)-plane in Figure 2(a). These are parameterized by the angular frequency ω as shown by the green and red arrows. The

curves for tangential stability (3.12) form lobes, and the angular frequency along the lobes changes from $\omega = \pi/2$ to $\omega \to \infty$, as shown by the green arrows in panel (a) and by the green curve in panel (b). Notice that the tips of the lobes are at $\omega \approx \pi$. For transversal stability, the boundaries (3.13) form a single horizontal curve in the (τ, κ)-plane. Along this curve the angular frequency varies in a narrow frequency domain around $\omega \approx \pi$, as shown by the red arrows in panel (a) and by the red oval in panels (b) and (c). The stability of the synchronized equilibrium changes via Andronov–Hopf bifurcation when crossing either a tangential or a transversal stability curve. That is, a pair of complex conjugate eigenvalues crosses the imaginary axis. The angular frequency of the arising oscillation is approximated by the imaginary part of the crossing roots ω. Depending on whether a tangential or a transversal stability curve is crossed, the arising spatiotemporal patterns will differ; in the former case the system remains synchronous, while in the latter case synchrony is broken.

Considering (3.10) and applying the analytical stability criteria in [50], it can be shown that the system is transversally stable within the leftmost lobe. Similar investigations for (3.11) reveal that the system is transversally stable above the wavy curve. For stability, both tangential and transversal stability are required; this requirement is only satisfied in the dashed domain in Figure 2(a). We remark that, when increasing the number of neurons, the lobes as well as the wavy curve move downward, while the "amplitude" of the wavy curve decreases. However, $N = 33$ is already very close to the limit $N \to \infty$; that is, no significant changes are observed when increasing N further.

Neural systems typically encode information using rhythmic patterns, which corresponds to periodic orbits. To obtain synchronous periodic solutions, one must solve (3.4) considering $[\, v_c(t) \;\; w_c(t) \,] = [\, v_c(t+T_p) \;\; w_c(t+T_p) \,]$, where T_p is the period of oscillations. When linearizing (3.1) about synchronous oscillations, the matrices (3.5) must be evaluated at the periodic orbits. In this case, L becomes time-dependent through $p(t) = -\frac{1}{C} h'(v_c(t))$, which appears in the modal equations (3.7) and (3.8). (For nonlinear coupling R would also be time-dependent.) By analyzing the corresponding monodromy operators one can determine the tangential and transversal stability of oscillations by calculating the location of the tangential and transversal Floquet multipliers; cf. (2.42) and (2.43) with $t = T_p$.

Figure 3 shows the peak-to-peak voltage amplitude of the oscillations when the time delay τ is varied. The corresponding value of the coupling constant is spelled out in each panel. Stable and unstable oscillations are depicted as green and red curves, respectively, and the same color code is used for the equilibrium (horizontal axis). Fold and pitchfork bifurcations (when a real multiplier crosses the unit circle at 1) are marked by crosses, while Neimark–Sacker bifurcations (when a complex conjugate pair of multipliers crosses the unit circle) are marked by stars. Blue and magenta symbols represent tangential and transversal stability losses.

For weak coupling (Figure 3(a)) the amplitude of oscillations does not change significantly with the delay, and stability is lost via transversal pitchfork bifurcations (magenta crosses). Branches of symmetry-breaking periodic solutions arise through these bifurcations (not shown in the figure) that correspond to cluster states. As the coupling strength is increased (Figure 3(b)), tangential fold bifurcations (blue crosses) appear for larger delay values, and the amplitude varies significantly with the delay. In particular, the amplitude of unstable oscillations decreases, which can also be observed in Figure 4, depicting stable and unstable

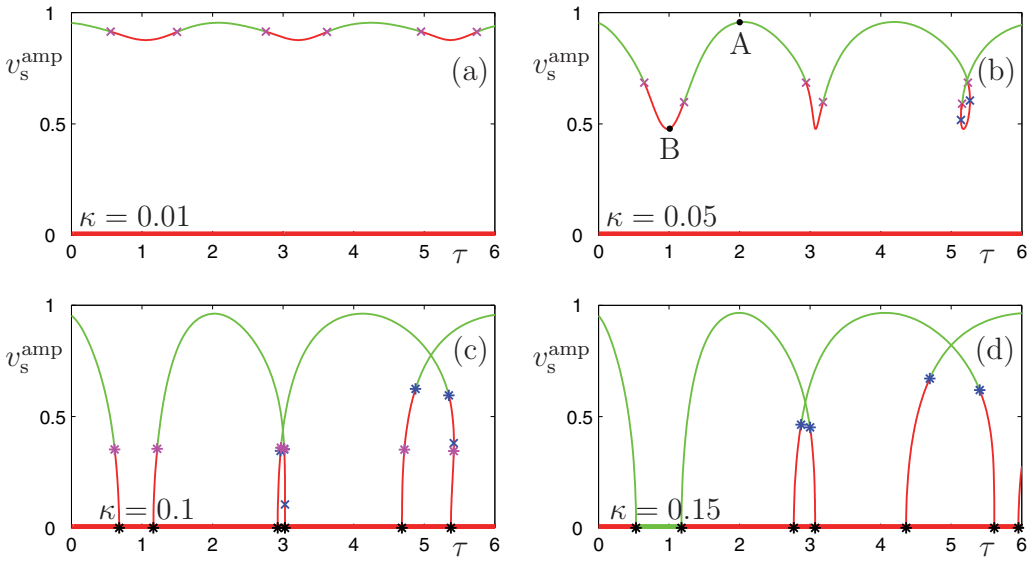

Figure 3. *Bifurcation diagrams showing the peak-to-peak voltage amplitude of synchronized oscillations as a function of the delay τ for different values of the coupling strength κ. The horizontal axis represents the equilibrium. Stable and unstable states are depicted by green and red curves. Black stars represent Hopf bifurcations of equilibria, while blue and magenta stars represent tangential and transversal Neimark–Sacker bifurcations of periodic orbits, respectively. Tangential fold and transversal pitchfork bifurcations are denoted by blue and magenta crosses, respectively.*

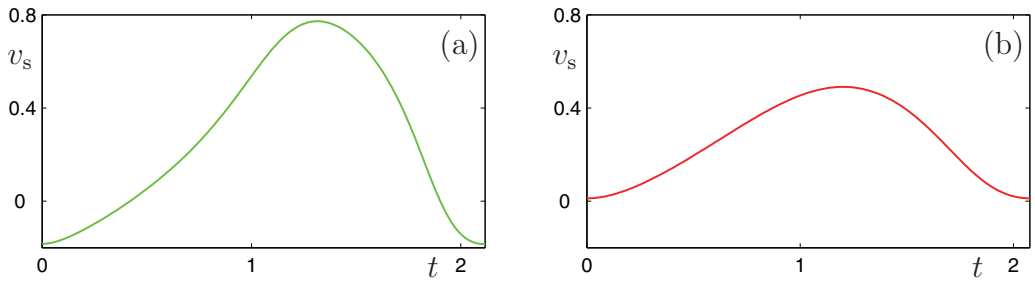

Figure 4. *Stable and unstable periodic orbits corresponding to the points* A *and* B *marked in Figure* 3(b).

oscillations corresponding to the points A and B. When the coupling strength exceeds the minimum of the lobes in Figure 2(a), the periodic branches "touch the ground" and connect to the equilibrium branch via Hopf bifurcations (black stars); see Figure 3(c). In this case both tangential and transversal stability losses occur mostly via Neimark–Sacker bifurcations (blue and magenta stars). At these bifurcations branches of quasi-periodic oscillations are created (not shown in the figure) that lead to more complicated spatiotemporal patterns. Finally, when the coupling strength exceeds the maximum of the wavy curve in Figure 2(a), all transversal bifurcations disappear, and only tangential Neimark–Sacker bifurcations remain; see Figure 3(d). For large delays the arising quasi-periodic oscillations may undergo further bifurcations, leading to synchronized chaos; see [11].

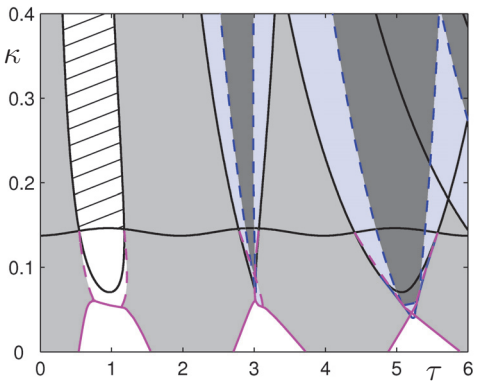

Figure 5. *Stability charts for synchronous periodic orbits. Black curves show the locations of Hopf bifurcations of the synchronized equilibrium, and in the dashed domain the equilibrium is stable; cf. Figure 2(a). Dashed blue and dashed magenta curves represent tangential and transversal Neimark–Sacker bifurcations, respectively. Solid blue curves represent tangential fold bifurcations, while solid magenta curves represent transversal pitchfork bifurcations. Light gray and dark gray regions correspond to having one stable and two stable synchronous oscillatory solutions, respectively, while stable and unstable oscillations coexist in the light blue domains.*

All bifurcations of synchronized equilibria and periodic orbits are summarized in Figure 5. Hopf bifurcations of the equilibrium are shown as black curves, and the domain where the equilibrium is stable is shown as dashed; cf. Figure 2(a). Tangential bifurcations of synchronous oscillations are shown as blue curves that are solid for fold and dashed for Neimark–Sacker bifurcations. Similarly, magenta curves represent transversal pitchfork (solid) and Neimark–Sacker (dashed) bifurcations. Notice that as κ is increased, the transversal bifurcations "switch" from pitchfork to Neimark–Sacker through bifurcations of higher codimension. In the white regions only unstable oscillations exist. Light gray regions contain one stable periodic orbit, while dark gray regions contain two stable periodic orbits. In the light blue regions stable and unstable oscillations coexist.

We remark that for weak coupling one might reduce system (3.1) to a systems of coupled phase oscillators; see [21]. However, this approach does not provide information about amplitude variations and, since the tangential dynamics is eliminated, only predicts transversal instabilities; see [33]. In fact, the phase oscillator model predicts the first trapezoidal domain in Figure 5 as a triangle, while in reality the top of the triangle is "chopped off."

3.2. Clustering of type II neurons. Let us consider the two-cluster states defined by $[\,v_i \;\; w_i\,] = [\,v_{c1} \;\; w_{c1}\,]$, $i = 1, \dots, b_1$, and $[\,v_i \;\; w_i\,] = [\,v_{c2} \;\; w_{c2}\,]$, $i = b_1 + 1, \dots, N$, of the type II neuromodel (3.1) with coupling (2.44). The corresponding two-cluster solutions are governed

by the system

(3.15)
$$
\begin{aligned}
C\dot{v}_{\mathrm{c}1}(t) &= h\big(v_{\mathrm{c}1}(t)\big) - w_{\mathrm{c}1}(t) + I + \frac{b_1-1}{N}\,\kappa\cdot\big(v_{\mathrm{c}1}(t-\tau) - v_{\mathrm{c}1}(t)\big) + \frac{b_2}{N}\,\kappa\cdot\big(v_{\mathrm{c}2}(t-\tau) - v_{\mathrm{c}1}(t)\big),\\
\dot{w}_{\mathrm{c}1}(t) &= v_{\mathrm{c}1}(t) - \gamma\, w_{\mathrm{c}1}(t),\\
C\dot{v}_{\mathrm{c}2}(t) &= h\big(v_{\mathrm{c}2}(t)\big) - w_{\mathrm{c}2}(t) + I + \frac{b_1}{N}\,\kappa\cdot\big(v_{\mathrm{c}1}(t-\tau) - v_{\mathrm{c}2}(t)\big) + \frac{b_2-1}{N}\,\kappa\cdot\big(v_{\mathrm{c}2}(t-\tau) - v_{\mathrm{c}2}(t)\big),\\
\dot{w}_{\mathrm{c}2}(t) &= v_{\mathrm{c}2}(t) - \gamma\, w_{\mathrm{c}2}(t).
\end{aligned}
$$

Indeed, the synchronous dynamics (3.4) is contained by the dynamics (3.15), which can be shown by setting $[\,v_{\mathrm{c}1}\ \ w_{\mathrm{c}1}\,] = [\,v_{\mathrm{c}2}\ \ w_{\mathrm{c}2}\,] = [\,v_{\mathrm{c}}\ \ w_{\mathrm{c}}\,]$.

When linearizing (3.1) about the two-cluster state, one obtains the matrices

$$
L_\ell = \begin{bmatrix} \frac{1}{C}h'(v_{\mathrm{c}\ell}) - \frac{N-1}{N}\frac{\kappa}{C} & -\frac{1}{C} \\ 1 & -\gamma \end{bmatrix}, \qquad R_{\ell k} = R = \begin{bmatrix} \frac{1}{N}\frac{\kappa}{C} & 0 \\ 0 & 0 \end{bmatrix}, \quad \ell, k = 1, 2; \tag{3.16}
$$

cf. (2.54), (2.56). Using the notation $z_1 = [\,\tilde{v}_{\mathrm{c}1}\ \ \tilde{w}_{\mathrm{c}1}\,]$, $z_2 = [\,\tilde{v}_{\mathrm{c}2}\ \ \tilde{w}_{\mathrm{c}2}\,]$, $z_i = [\,\tilde{v}_{\mathrm{b}1}\ \ \tilde{w}_{\mathrm{b}1}\,]$, $i = 3, \dots, b_1+1$, and $z_i = [\,\tilde{v}_{\mathrm{b}2}\ \ \tilde{w}_{\mathrm{b}2}\,]$, $i = b_1+2, \dots, N$, the first equation in (2.56) results in

$$
\begin{aligned}
\begin{bmatrix} \dot{\tilde{v}}_{\mathrm{c}1}(t) \\ \dot{\tilde{w}}_{\mathrm{c}1}(t) \\ \dot{\tilde{v}}_{\mathrm{c}2}(t) \\ \dot{\tilde{w}}_{\mathrm{c}2}(t) \end{bmatrix} &= \left[\begin{array}{cc:cc} -p_1 - q & -\frac{1}{C} & 0 & 0 \\ 1 & -\gamma & 0 & 0 \\ \hdashline 0 & 0 & -p_2 - q & -\frac{1}{C} \\ 0 & 0 & 1 & -\gamma \end{array}\right] \begin{bmatrix} \tilde{v}_{\mathrm{c}1}(t) \\ \tilde{w}_{\mathrm{c}1}(t) \\ \tilde{v}_{\mathrm{c}2}(t) \\ \tilde{w}_{\mathrm{c}2}(t) \end{bmatrix} \\
&\quad + \left[\begin{array}{cc:cc} (b_1-1)r & 0 & b_2 r & 0 \\ 0 & 0 & 0 & 0 \\ \hdashline b_1 r & 0 & (b_2-1)r & 0 \\ 0 & 0 & 0 & 0 \end{array}\right] \begin{bmatrix} \tilde{v}_{\mathrm{c}1}(t-\tau) \\ \tilde{w}_{\mathrm{c}1}(t-\tau) \\ \tilde{v}_{\mathrm{c}2}(t-\tau) \\ \tilde{w}_{\mathrm{c}2}(t-\tau) \end{bmatrix},
\end{aligned} \tag{3.17}
$$

which is the linearization of (3.15), while the remaining equations in (2.56) yield

$$
\begin{aligned}
\begin{bmatrix} \dot{\tilde{v}}_{\mathrm{b}1}(t) \\ \dot{\tilde{w}}_{\mathrm{b}1}(t) \end{bmatrix} &= \begin{bmatrix} -p_1 - q & -\frac{1}{C} \\ 1 & -\gamma \end{bmatrix} \begin{bmatrix} \tilde{v}_{\mathrm{b}1}(t) \\ \tilde{w}_{\mathrm{b}1}(t) \end{bmatrix} + \begin{bmatrix} -r & 0 \\ 0 & 0 \end{bmatrix} \begin{bmatrix} \tilde{v}_{\mathrm{b}1}(t-\tau) \\ \tilde{w}_{\mathrm{b}1}(t-\tau) \end{bmatrix}, \\
\begin{bmatrix} \dot{\tilde{v}}_{\mathrm{b}2}(t) \\ \dot{\tilde{w}}_{\mathrm{b}2}(t) \end{bmatrix} &= \begin{bmatrix} -p_2 - q & -\frac{1}{C} \\ 1 & -\gamma \end{bmatrix} \begin{bmatrix} \tilde{v}_{\mathrm{b}2}(t) \\ \tilde{w}_{\mathrm{b}2}(t) \end{bmatrix} + \begin{bmatrix} -r & 0 \\ 0 & 0 \end{bmatrix} \begin{bmatrix} \tilde{v}_{\mathrm{b}2}(t-\tau) \\ \tilde{w}_{\mathrm{b}2}(t-\tau) \end{bmatrix},
\end{aligned} \tag{3.18}
$$

where

$$
\begin{aligned}
p_1 &= -\frac{1}{C}h'(v_{\mathrm{c}1}), \quad p_2 = -\frac{1}{C}h'(v_{\mathrm{c}2}),\\
q &= \frac{N-1}{N}\frac{\kappa}{C}, \qquad r = \frac{1}{N}\frac{\kappa}{C}.
\end{aligned} \tag{3.19}
$$

Using (3.17), (3.18), (3.19), one may study the tangential and transversal stability of cluster equilibria $[\,v_{\mathrm{c}1}(t)\ \ w_{\mathrm{c}1}(t)\ \ v_{\mathrm{c}2}(t)\ \ w_{\mathrm{c}2}(t)\,] \equiv [\,v^*_{\mathrm{c}1}\ \ w^*_{\mathrm{c}1}\ \ v^*_{\mathrm{c}2}\ \ w^*_{\mathrm{c}2}\,]$, which can be derived from (3.15). For the example considered here the only equilibrium is the synchronized one

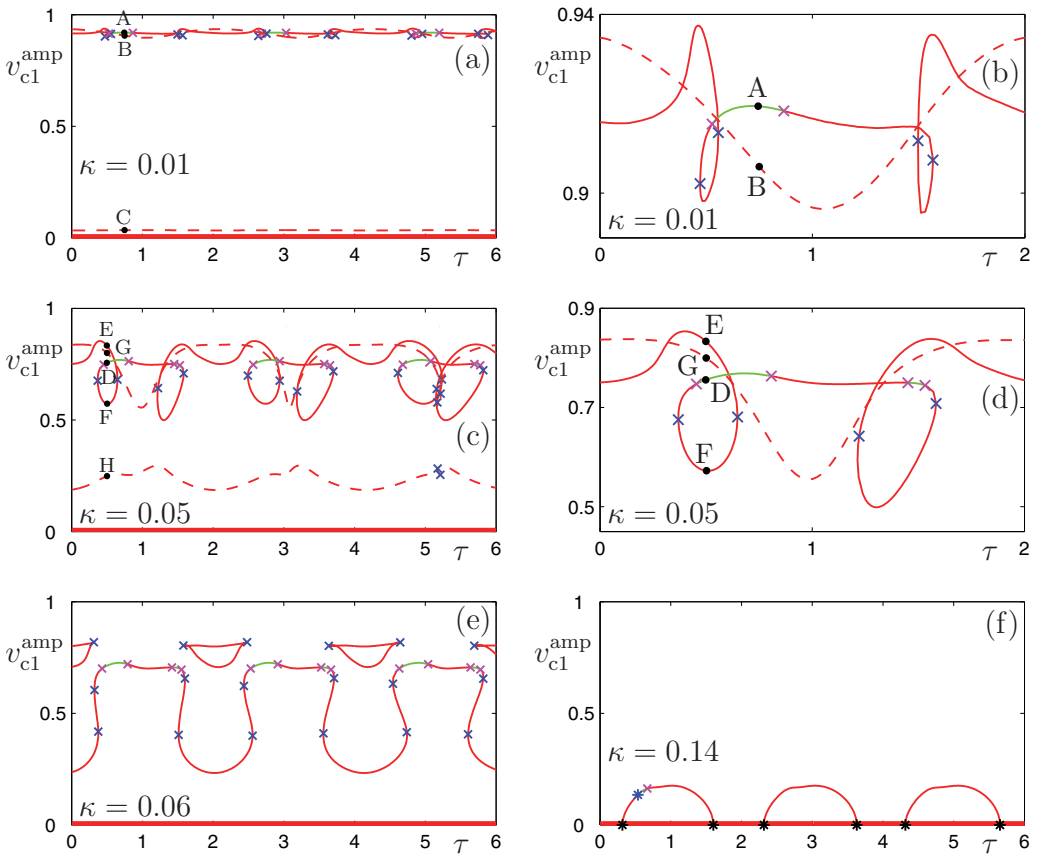

Figure 6. *Bifurcation diagrams showing the peak-to-peak voltage amplitude of the first cluster for two-cluster states with* $[b_1 \;\; b_2] = [17 \;\; 16]$. *The same notation and color-coding are used as in Figure 3.*

$v_{c1}^* = v_{c2}^* = v_c^*$, $w_{c1}^* = w_{c2}^* = w_c^*$ that has already been explained above. For periodic solutions the coefficient matrices of the nondelayed terms become time-dependent via $p_1(t) = -\frac{1}{C}h'(v_{c1}(t))$, $p_2(t) = -\frac{1}{C}h'(v_{c2}(t))$ in (3.17), (3.18). Similarly to the case of synchronized oscillations, we use numerical continuation to analyze oscillatory two-cluster solutions. For $b_1 = b_2$ one can observe "phase-locked" solutions where the time profiles of oscillations of different clusters differ only in phase. The theory of weakly coupled systems [18] suggests that "phase-locked" solutions exist for $b_1 \neq b_2$, so that the phase shift changes with the ratio b_1/b_2. As a matter of fact, we found this to be only approximately true: the time profiles for each cluster differ slightly. We refer to these solutions as "phase-locked-like" solutions. Moreover, we found that there also exist additional solutions where the time profiles of the two clusters differ significantly. Such states cannot be obtained using the weakly coupled approximation. For the results presented below we choose the number of neurons to be $N = 33$ so that $b_1 = 17$ and $b_2 = 16$ oscillators are contained by the clusters.

The peak-to-peak voltage amplitude of oscillations for the first cluster is shown in Figure 6, where the same notation and color-coding as in Figure 3 are used. In order to help the readability of the figures, we do not show bifurcations that occur where the branch is already

unstable (with the exception of where the branches fold). Note that tangential and transversal stability is understood here with respect to the two-cluster states.

For weak coupling (Figure 6(a),(b)) there exist three distinct branches of oscillatory solutions. The branch shown as a continuous curve corresponds to phase-locked-like solutions. These are depicted in Figure 7(a) for point A where blue and magenta curves correspond to the first and the second clusters, respectively. The amplitude variations in Figure 6(a),(b) are small and become smaller when $\kappa \to 0$ while keeping the general folding structure. We also remark that the inner pair of fold bifurcations for each loop pair corresponds to the bifurcations in Figure 3(a); that is, the two-cluster states bifurcate from the synchronized solution by symmetry breaking. The section of the top branch between the outer pair of fold bifurcations is in fact tangentially stable, but only a smaller section of it is transversally stable. Dashed branches correspond to asymmetric solutions where the oscillations within one cluster have much larger amplitude compared to the other cluster, as shown in Figure 7(b) and (c) for the points B and C. When $\kappa \to 0$, the smaller amplitude goes to zero, which results in solutions where one cluster oscillates while the other exhibits equilibrium.

As the coupling strength is increased (Figure 6(c),(d)) the amplitude variations increase. As shown in Figure 7(d), (e), and (f) for points D, E, and F, the middle part of the continuous branch still represents the phase-locked-like solutions, while for the loop the oscillations become more asymmetric. At the same time, the dashed branches become less asymmetric, as can be observed in Figure 7(g) and (h), which represent the oscillations for points G and H. When increasing κ further, the branches of asymmetric oscillations "meet", and a sequence of higher codimension bifurcations leads to a new type of behavior shown in Figure 6(e). For even stronger coupling, the separated loops disappear, while the "tooth-like" branch "touches the ground" and connects to the equilibrium through Hopf bifurcations; see Figure 6(f). These Hopf bifurcations correspond to the horizontal wavy curve in Figure 2. When κ is larger than the maximum of this curve, the periodic two-cluster solutions disappear.

The two-dimensional bifurcation diagram in Figure 8 summarizes the behavior in the (τ, κ) parameter plane. The notation and color-coding are adopted from Figure 5. One may observe that the shaded domain (where a stable two-cluster solution exists) is bounded by tangential as well as transversal bifurcation curves. Solid blue curves correspond to branch folding, while dashed blue curves show the location of the birth of quasi-periodic two-cluster states through Neimark–Sacker bifurcations. Transversal pitchfork bifurcations that lead to oscillatory cluster states with more than two clusters are depicted as solid magenta curves.

4. Conclusion and discussion.

The dynamics of delayed networks with nonlinear elements and nonlinear coupling were studied in this paper. It was shown that around a cluster state, the nonlinear coupling introduces heterogeneity into the linearized system. A theorem was stated that gave conditions on the intracluster and intercluster connectivity that allow decomposition around cluster states with nonequal cluster sizes (and possibly different dynamics in each cluster). Moreover, a decomposition method was presented that created modal subsystems of clear physical meaning and allowed us to investigate the dynamics in the vicinity of steady and oscillatory cluster states. It was shown that with the appropriate relaxation of conditions

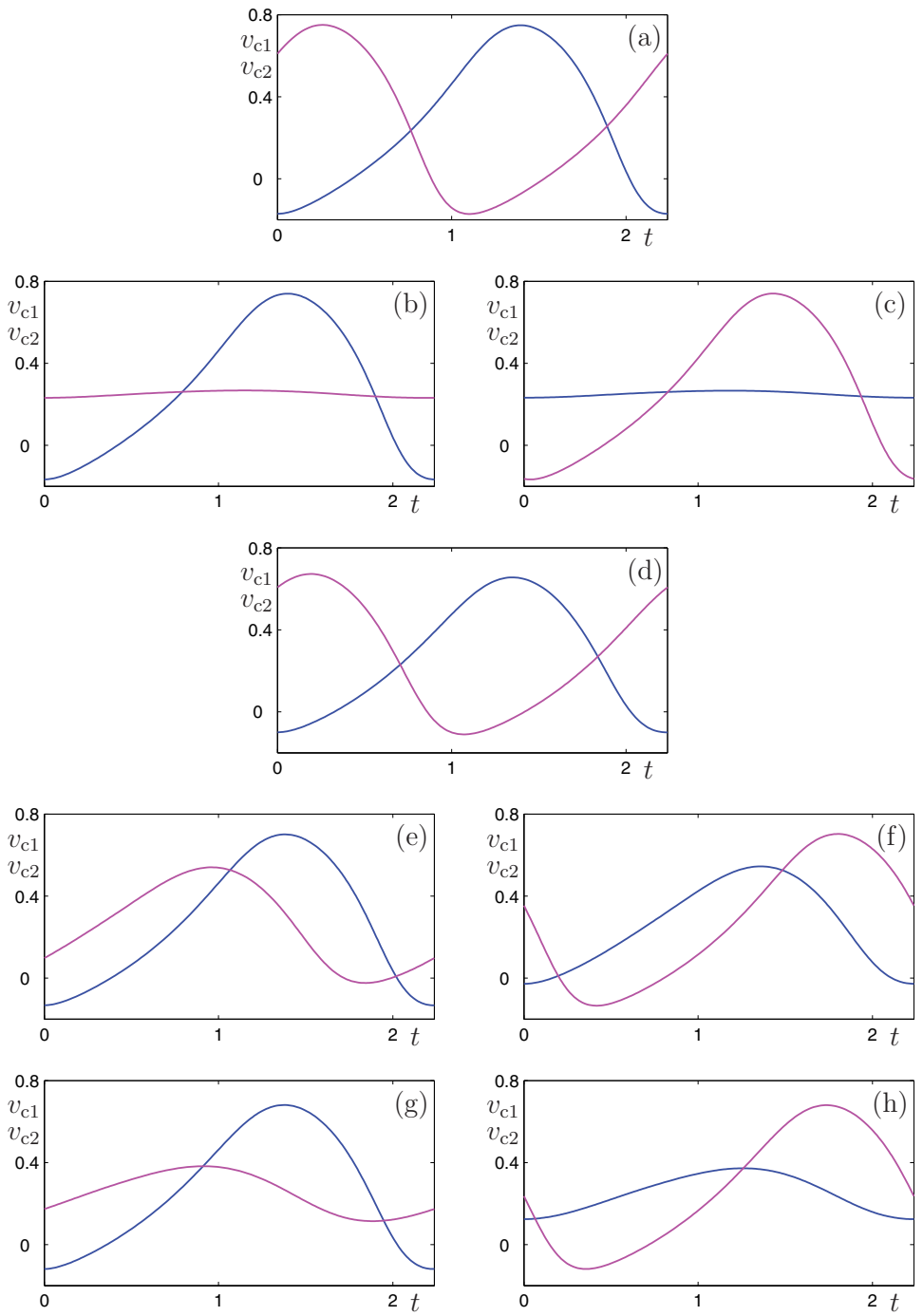

Figure 7. *Time profiles of the oscillations for the first and second clusters (blue and magenta) are shown corresponding to the points marked* A–H *in Figure* 4(a)–(d). *Notice that panels* (a) *and* (d) *depict the "phase-locked like" solutions, while in all other panels the oscillations for the individual clusters differ significantly.*

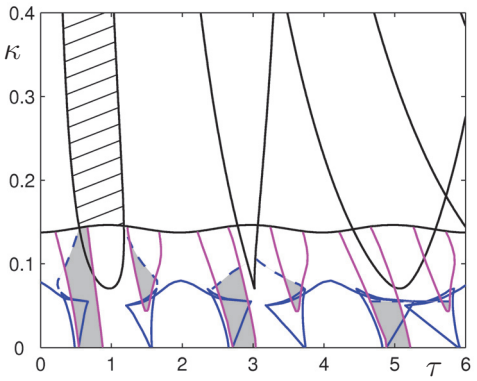

Figure 8. *Stability charts for two-cluster solutions. The same notation of curves is used as in Figure 5. The light gray shading represents the regions with a stable two-cluster state.*

in the decomposability theorem, the proposed transformations can be used to derive an upper block triangular form that simplifies the stability analysis significantly. The corresponding restrictions on the network connectivity were formalized in another theorem. We used the obtained modal equations to derive exact stability conditions for cluster equilibria and periodic orbits. For cluster equilibria, stability charts were derived analytically using the D-subdivision method, while for cluster oscillations charts were drawn using Floquet theory. The methods presented can be used for networked nonlinear systems of realistic size and allow one to map out the skeleton of the dynamics consisting of stable and unstable states even when a large number of different cluster configurations coexist.

The methods were applied to a neurosystem where cluster oscillations are used to encode information and perform neurocomputation. It was shown that for weak coupling the synchronous oscillations lose stability by splitting into smaller clusters, while for stronger coupling more complicated synchronous motions (e.g., quasi-periodic oscillations) may appear. When analyzing cluster oscillations, it was shown that, despite common beliefs supported by phase oscillator models, no exact phase-locked solutions exist for nonequal cluster sizes. Indeed, some oscillations remain "phase-locked-like", but strongly asymmetric cluster oscillations also exist where the motion of each cluster differs significantly. Even "mixed" cluster states were discovered where some clusters stop oscillating and return to equilibria. These results shed some light on the mechanism of neural coding via cluster states and show the limitation of the phase oscillator approach. In the future, we plan to apply these methods to systems with different neural models and connectivity [39] and study the effect of heterogeneities in nonlinear delayed networks [53].

Appendix A. Identifying cluster states. Let us recall the adjacency matrices (2.26), (2.38):

$$A_7 = \begin{bmatrix} 0 & 0 & 1 & 1 & 1 & 1 & 1 \\ 1 & 0 & 0 & 1 & 1 & 1 & 1 \\ 0 & 1 & 0 & 1 & 1 & 1 & 1 \\ 1 & 1 & 1 & 0 & 0 & 1 & 1 \\ 1 & 1 & 1 & 1 & 0 & 0 & 1 \\ 1 & 1 & 1 & 1 & 1 & 0 & 0 \\ 1 & 1 & 1 & 0 & 1 & 1 & 0 \end{bmatrix}, \qquad A_7 = \begin{bmatrix} 0 & 0 & 1 & 1 & 0 & 1 & 1 \\ 1 & 0 & 0 & 1 & 1 & 0 & 1 \\ 0 & 1 & 0 & 1 & 1 & 1 & 0 \\ 1 & 0 & 0 & 0 & 1 & 1 & 0 \\ 1 & 0 & 0 & 1 & 0 & 1 & 0 \\ 1 & 0 & 0 & 1 & 0 & 0 & 1 \\ 1 & 0 & 0 & 1 & 1 & 0 & 0 \end{bmatrix}. \tag{A.1}$$

By using the Stirling number of the second kind (2.7) one can calculate the number of admissible cluster configurations that are listed in the second column of Table 1. The admissible configurations can be found by using a set partitioning algorithm [29]. By checking the corresponding subrow sums (2.6), one can identify the realizable cluster configurations shown in the last two columns of Table 1. Notice that in both cases the two-cluster configuration $\{1,2,3\},\{4,5,6,7\}$ can be realized, implying that there exists a corresponding clustering manifold (2.4) in state space. In the case of the first example, the system remains invariant when cyclically permuting the first three and the last four elements, and there exists a corresponding permutation matrix P_7 such that $P_7 A_7 P_7^{-1} = A_7$. On the other hand, for the second example, no such matrix can be found, and thus, identifying the symmetry becomes much more difficult; see Lemma 3 in [51]. The set partitioning algorithm [29] can be used for up to approximately 20 oscillators on a standard desktop computer to identify all admissible and the realizable cluster configurations, while identifying all symmetries for systems of this size with general coupling structure may be difficult. Indeed, for large numbers of oscillators, the number of cluster states becomes very large, and thus both symmetry-based and set decomposition methods become computationally expensive.

Table 1
Cluster configurations for examples (A.1).

	# of admissible clusters	Example 1	Example 2
Synchrony	$S(7,1)=1$	$\{1,2,3,4,5,6,7\}$	—
Two-clusters	$S(7,2)=63$	$\{1,2,3\},\{4,5,6,7\}$	$\{1,2,3\},\{4,5,6,7\}$
Three-clusters	$S(7,3)=301$	$\{1,2,3\},\{4,6\},\{5,7\}$	$\{1,2,3\},\{4\},\{5,6,7\}$
Four-clusters	$S(7,4)=350$	$\{1\},\{2\},\{3\},\{4,5,6,7\}$	$\{1\},\{2\},\{3\},\{4,5,6,7\}$
Five-clusters	$S(7,5)=140$	$\{1,2,3\},\{4\},\{5\},\{6\},\{7\}$ $\{1\},\{2\},\{3\},\{4,6\},\{5,7\}$	$\{1\},\{2\},\{3\},\{4\},\{5,6,7\}$
Six-clusters	$S(7,6)=21$	—	$\{1\},\{2\},\{3\},\{4,5\},\{6\},\{7\}$
Splay state	$S(7,7)=1$	$\{1\},\{2\},\{3\},\{4\},\{5\},\{6\},\{7\}$	$\{1\},\{2\},\{3\},\{4\},\{5\},\{6\},\{7\}$
All	$B(7)=877$		

Appendix B. Proof of Theorem 1. Here we show why conditions (2.17), (2.18) are required to be able to decompose the system using the transformation (2.19), (2.20), (2.21). Notice that investigating the effects of $T_N^K \otimes I$ on (2.16) is equivalent to investigating the effects of T_N^K on the system where the n-dimensional matrices L_ℓ and $R_{\ell k}$ are substituted by the scalars l_ℓ and $r_{\ell k}$, respectively. That is, one needs to study the effects of T_N^K on a

system with matrices $(I_N \otimes l_\ell)$ and $(A_N \otimes r_{\ell k})$ in front of the delayed and nondelayed terms, respectively.

The first K rows of the inverse transformation are given by

$$\left(T_N^K\right)^{-1}_{ij} = \begin{cases} \frac{1}{b_\ell} & \text{if} \quad i = \ell \quad \text{and} \quad j = B_{\ell-1}+1, \dots, B_\ell, \\ 0 & \text{otherwise} \end{cases} \tag{B.1}$$

for $\ell = 1, \dots, K$, and the remaining $N-K$ rows are defined as

$$\left(T_N^K\right)^{-1}_{ij} = \begin{cases} \frac{b_\ell - 1}{b_\ell} & \text{if} \quad i = K + B_{\ell-1} - (\ell-1) + p \quad \text{and} \quad j = B_{\ell-1} + 1 + p, \\ \frac{1}{b_\ell} & \text{if} \quad i = K + B_{\ell-1} - (\ell-1) + p \quad \text{and} \quad j = B_{\ell-1} + q, \qquad q \neq 1+p, \\ 0 & \text{otherwise} \end{cases} \tag{B.2}$$

for $p, q = 1, \dots, b_\ell - 1$, $\ell = 1, \dots, K$. For example, the inverse of (2.28) becomes

$$(T_7^2)^{-1} = \left[\begin{array}{ccc:cccc} \frac{1}{3} & \frac{1}{3} & \frac{1}{3} & 0 & 0 & 0 & 0 \\ 0 & 0 & 0 & \frac{1}{4} & \frac{1}{4} & \frac{1}{4} & \frac{1}{4} \\ \hdashline \frac{1}{3} & -\frac{2}{3} & \frac{1}{3} & 0 & 0 & 0 & 0 \\ \frac{1}{3} & \frac{1}{3} & -\frac{2}{3} & 0 & 0 & 0 & 0 \\ \hdashline 0 & 0 & 0 & \frac{1}{4} & -\frac{3}{4} & \frac{1}{4} & \frac{1}{4} \\ 0 & 0 & 0 & \frac{1}{4} & \frac{1}{4} & -\frac{3}{4} & \frac{1}{4} \\ 0 & 0 & 0 & \frac{1}{4} & \frac{1}{4} & \frac{1}{4} & -\frac{3}{4} \end{array}\right]. \tag{B.3}$$

It is easy to show that $\left(T_N^K\right)^{-1}(I_N \otimes l_\ell)\, T_N^K$ is still diagonal and only the order of the diagonal elements changes; see (2.29). What remains to be shown is that $\left(T_N^K\right)^{-1}(A_N \otimes r_{\ell k})\, T_N^K$ will separate the tangential and transversal dynamics. First, we show that the $r_{\ell\ell}$ do not appear outside the K-dimensional tangential block and the $b_\ell - 1$-dimensional transversal block located at the diagonal; see (2.30). The terms in these blocks originate from

$$\begin{bmatrix} \frac{1}{b_\ell} & \cdots & \frac{1}{b_\ell} \end{bmatrix} \left[r_{\ell\ell}\right] \begin{bmatrix} 1 \\ \vdots \\ 1 \end{bmatrix} \tag{B.4}$$

and

$$\begin{bmatrix} \frac{1}{b_\ell} & \cdots & \frac{b_\ell - 1}{b_\ell} & \cdots & \frac{1}{b_\ell} \end{bmatrix} \left[r_{\ell\ell}\right] \begin{bmatrix} 1 \\ 0 \\ \vdots \\ -1 \\ \vdots \\ 0 \end{bmatrix}, \tag{B.5}$$

respectively, where $\left[r_{\ell\ell}\right]$ denotes the $b_\ell \times b_\ell$ block. Moreover, due to the constant subrow sum

condition (2.6), the off-diagonal terms

$$\begin{bmatrix} \frac{1}{b_\ell} & \cdots & \frac{b_\ell - 1}{b_\ell} & \cdots & \frac{1}{b_\ell} \end{bmatrix} \begin{bmatrix} r_{\ell\ell} \end{bmatrix} \begin{bmatrix} 1 \\ \vdots \\ 1 \end{bmatrix} = 0 \tag{B.6}$$

disappear. Similarly, the terms given by

$$\begin{bmatrix} \frac{1}{b_\ell} & \cdots & \frac{1}{b_\ell} \end{bmatrix} \begin{bmatrix} r_{\ell\ell} \end{bmatrix} \begin{bmatrix} 1 \\ 0 \\ \vdots \\ -1 \\ \vdots \\ 0 \end{bmatrix} = 0 \tag{B.7}$$

are eliminated by the constant subcolumn sum condition in (2.17). Notice that (B.6) and (B.7) mean that the corresponding b_ℓ-dimensional vectors are orthogonal through the $b_\ell \times b_\ell$ block $\begin{bmatrix} r_{\ell\ell} \end{bmatrix}$.

We also need to show that the elements $r_{\ell k}$, $\ell \neq k$, do not appear outside the K-dimensional tangential block (2.30). The elements in this block are given by

$$\begin{bmatrix} \frac{1}{b_\ell} & \cdots & \frac{1}{b_\ell} \end{bmatrix} \begin{bmatrix} r_{\ell k} \end{bmatrix} \begin{bmatrix} 1 \\ \vdots \\ 1 \end{bmatrix}, \tag{B.8}$$

where $\begin{bmatrix} r_{\ell k} \end{bmatrix}$ denotes the $b_\ell \times b_k$ block, while the orthogonality condition

$$\begin{bmatrix} \frac{1}{b_\ell} & \cdots & \frac{b_\ell - 1}{b_\ell} & \cdots & \frac{1}{b_\ell} \end{bmatrix} \begin{bmatrix} r_{\ell k} \end{bmatrix} \begin{bmatrix} 1 \\ \vdots \\ 1 \end{bmatrix} = 0 \tag{B.9}$$

is satisfied due to the constant subrow sum condition; cf. (2.6). To eliminate the remaining off-diagonal terms, we require the orthogonality

$$\begin{bmatrix} \frac{1}{b_\ell} & \cdots & \frac{b_\ell - 1}{b_\ell} & \cdots & \frac{1}{b_\ell} \end{bmatrix} \begin{bmatrix} r_{\ell k} \end{bmatrix} \begin{bmatrix} 1 \\ 0 \\ \vdots \\ -1 \\ \vdots \\ 0 \end{bmatrix} = 0, \tag{B.10}$$

which holds if each column in the block $\begin{bmatrix} r_{\ell k} \end{bmatrix}$ is either full of zeros or full of ones. Finally, we

also require that

$$\begin{bmatrix} \frac{1}{b_\ell} & \cdots & \frac{1}{b_\ell} \end{bmatrix} \begin{bmatrix} r_{\ell k} \end{bmatrix} \begin{bmatrix} 1 \\ 0 \\ \vdots \\ -1 \\ \vdots \\ 0 \end{bmatrix} = 0, \tag{B.11}$$

which is satisfied if the subcolumn sums are the same. Combining the last two conditions yields that the whole $b_\ell \times b_k$ block $\begin{bmatrix} r_{\ell k} \end{bmatrix}$ must be either full of zeros or full of ones, which completes the proof of Theorem 1.

We remark that the matrices

(B.12)

$$\left[\begin{array}{ccc:cccc} 0 & 0 & 1 & 1 & 1 & 1 & 1 \\ 1 & 0 & 0 & 1 & 1 & 1 & 1 \\ 0 & 1 & 0 & 1 & 1 & 1 & 1 \\ \hdashline 0 & 0 & 0 & 0 & 0 & 1 & 1 \\ 0 & 0 & 0 & 1 & 0 & 0 & 1 \\ 0 & 0 & 0 & 1 & 1 & 0 & 0 \\ 0 & 0 & 0 & 0 & 1 & 1 & 0 \end{array}\right], \quad \left[\begin{array}{ccc:cccc} 0 & 0 & 1 & 0 & 0 & 0 & 0 \\ 1 & 0 & 0 & 0 & 0 & 0 & 0 \\ 0 & 1 & 0 & 0 & 0 & 0 & 0 \\ \hdashline 1 & 1 & 1 & 0 & 0 & 1 & 1 \\ 1 & 1 & 1 & 1 & 0 & 0 & 1 \\ 1 & 1 & 1 & 1 & 1 & 0 & 0 \\ 1 & 1 & 1 & 0 & 1 & 1 & 0 \end{array}\right], \quad \left[\begin{array}{ccc:cccc} 0 & 0 & 1 & 0 & 0 & 0 & 0 \\ 1 & 0 & 0 & 0 & 0 & 0 & 0 \\ 0 & 1 & 0 & 0 & 0 & 0 & 0 \\ \hdashline 0 & 0 & 0 & 0 & 0 & 1 & 1 \\ 0 & 0 & 0 & 1 & 0 & 0 & 1 \\ 0 & 0 & 0 & 1 & 1 & 0 & 0 \\ 0 & 0 & 0 & 0 & 1 & 1 & 0 \end{array}\right]$$

satisfy Theorem 1 and differ only in their intercluster connectivity when compared to (2.26). They allow decomposition similar to that in section 2.2, and only the tangential dynamics change in the decomposed system according to

$$\begin{bmatrix} R_{11} & 4R_{12} \\ 0 & 2R_{22} \end{bmatrix}, \quad \begin{bmatrix} R_{11} & 0 \\ 3R_{21} & 2R_{22} \end{bmatrix}, \quad \begin{bmatrix} R_{11} & 0 \\ 0 & 2R_{22} \end{bmatrix}; \tag{B.13}$$

cf. (2.30), (2.31).

Acknowledgments. The author thanks Steve Coombes very much for providing inspiration for this work and gratefully acknowledges discussions with Feng Wei, Galip Ulsoy, and Gábor Stépán.

REFERENCES

[1] P. Ashwin and J. W. Swift, *The dynamics of n weakly coupled identical oscillators*, J. Nonlinear Sci., 2 (1992), pp. 69–108.

[2] H. Aufderheide, L. Rudolf, and T. Gross, *Mesoscale symmetries explain dynamical equivalence of food webs*, New J. Phys., 14 (2012), 105014.

[3] K. B. Blyuss and Y. N. Kyrychko, *Symmetry breaking in a model of antigenic variation with immune delay*, Bull. Math. Biol., 74 (2012), pp. 2488–2509.

[4] S. A. Campbell, *Time delays in neural systems*, in Handbook of Brain Connectivity, Understanding Complex Systems, V. K. Jirsa and A. R. McIntosh, eds., Springer, New York, 2007, pp. 65–90.

[5] S. A. Campbell and I. Kobelevskiy, *Phase models and oscillators with time delayed coupling*, Discrete Contin. Dynam. Syst., 32 (2012), pp. 2653–2673.

[6] R. Cepeda-Gomez and N. Olgac, *An exact method for the stability analysis of linear consensus protocols with time delay*, IEEE Trans. Automat. Control, 56 (2011), pp. 1734–1740.
[7] C.-U. Choe, T. Dahms, P. Hövel, and E. Schöll, *Controlling synchrony by delay coupling in networks: From in-phase to splay and cluster states*, Phys. Rev. E, 81 (2010), 025205.
[8] S. Coombes, *Neuronal networks with gap junctions: A study of piecewise linear planar neuron models*, SIAM J. Appl. Dyn. Syst., 7 (2008), pp. 1101–1129.
[9] S. Coombes and C. Laing, *Delays in activity-based neural networks*, Philos. Trans. R. Soc. Lond. Ser. A Math. Phys. Eng. Sci., 367 (2009), pp. 1117–1129.
[10] T. Dahms, J. Lehnert, and E. Schöll, *Cluster and group synchronization in delay-coupled networks*, Phys. Rev. E, 86 (2012), 016202.
[11] O. D'Huys, I. Fischer, J. Danckaert, and R. Vicente, *Role of delay for the symmetry in the dynamics of networks*, Phys. Rev. E, 83 (2011), 046223.
[12] B. Dionne, M. Golubitsky, and I. Stewart, *Coupled cells with internal symmetry:* I. *Wreath products*, Nonlinearity, 9 (1996), pp. 559–574.
[13] B. Dionne, M. Golubitsky, and I. Stewart, *Coupled cells with internal symmetry:* II. *Direct products*, Nonlinearity, 9 (1996), pp. 575–599.
[14] A.-L. Do, J. Hoefener, and T. Gross, *Engineering mesoscale structures with distinct dynamical implications*, New J. Phys., 14 (2012), 115022.
[15] B. Ermentrout and T.-W. Ko, *Delays and weakly coupled neuronal oscillators*, Philos. Trans. R. Soc. Lond. Ser. A Math. Phys. Eng. Sci., 367 (2009), pp. 1097–1115.
[16] G. B. Ermentrout and D. H. Terman, *Mathematical Foundations of Neuroscience*, Interdiscip. Appl. Math. 35, Springer, New York, 2010.
[17] V. Flunkert, S. Yanchuk, T. Dahms, and E. Schöll, *Synchronizing distant nodes: A universal classification of networks*, Phys. Rev. Lett., 105 (2010), 254101.
[18] F. C. Hoppensteadt and E. M. Izhikevich, *Dynamical Systems in Neuroscience: The Geometry of Excitability and Bursting*, Appl. Math. Sci. 126, Springer, New York, 1997.
[19] T. Insperger and G. Stépán, *Semi-discretization for Time-Delay Systems: Stability and Engineering Applications*, Appl. Math. Sci. 178, Springer, New York, 2011.
[20] D. Irving and F. Sorrentino, *Synchronization of dynamical hypernetworks: Dimensionality reduction through simultaneous block-diagonalization of matrices*, Phys. Rev. E, 86 (2012), 056102.
[21] E. M. Izhikevich, *Phase models with explicit time delays*, Phys. Rev. E, 58 (1998), pp. 905–908.
[22] E. M. Izhikevich, *Polysynchronization: Computation with spikes*, Neural Comput., 18 (2006), pp. 245–282.
[23] E. M. Izhikevich, *Dynamical Systems in Neuroscience: The Geometry of Excitability and Bursting*, MIT Press, Cambridge, MA, 2007.
[24] A. Kesting and M. Treiber, *How reaction time, update time, and adaptation time influence the stability of traffic flow*, Comput. Aided Civil Infrastructure Engrg., 23 (2008), pp. 125–137.
[25] W. Kinzel, A. Englert, G. Reents, M. Zigzag, and I. Kanter, *Synchronization of networks of chaotic units with time-delayed couplings*, Phys. Rev. E, 79 (2009), 056207.
[26] K. Konishia, L. B. Le, and N. Hara, *Stabilization of a steady state in oscillators coupled by a digital delayed connection*, European Phys. J., 85 (2012), 166.
[27] J. Lehnert, T. Dahms, P. Hövel, and E. Schöll, *Loss of synchronization in complex neuronal networks with delay*, European Phys. Lett., 96 (2011), 60013.
[28] P. Lin and Y. Jia, *Consensus of second-order discrete-time multi-agent systems with nonuniform time-delays and dynamically changing topologies*, Automatica J. IFAC, 45 (2009), pp. 2154–2158.
[29] B. Luong, *Set Partition*, Tech. report, http://www.mathworks.com/matlabcentral/fileexchange/24133-set-partition, 2009.
[30] Z. Meng, W. Ren, Y. Cao, and Z. You, *Leaderless and leader-following consensus with communication and input delays under a directed network topology*, IEEE Trans. Syst. Man Cybernet. B, 41 (2011), pp. 75–88.
[31] W. Michiels and H. Nijmeijer, *Synchronization of delay-coupled nonlinear oscillators: An approach based on the stability analysis of synchronized equilibria*, Chaos, 19 (2009), 033110.
[32] J. L. Mitchell and T. W. Carr, *Synchronous versus asynchronous oscillations for antigenically varying* Plasmodium falciparum *with host immune response*, J. Biol. Dynam., 6 (2012), pp. 333–357.

[33] E. Montbrió, D. Pazó, and J. Schmidt, *Time delay in the Kuramoto model with bimodal frequency distribution*, Phys. Rev. E, 74 (2006), 056201.
[34] J. von Neumann, *The Computer and the Brain*, Yale University Press, New Haven, CT, 1958.
[35] M. Newman, A.-L. Barabasi, and D. J. Watts, *The Structure and Dynamics of Networks*, Princeton University Press, Princeton, NJ, 2006.
[36] V. Novičenko and K. Pyragas, *Phase reduction of weakly perturbed limit cycle oscillations in time-delay systems*, Phys. D, 241 (2012), pp. 1090–1098.
[37] R. Olfati-Saber, J. A. Fax, and R. M. Murray, *Consensus and cooperation in networked multi-agent systems*, Proc. IEEE, 95 (2007), pp. 215–233.
[38] R. Olfati-Saber and R. M. Murray, *Consensus problems in networks of agents with switching topology and time-delays*, IEEE Trans. Automat. Control, 49 (2004), pp. 1520–1533.
[39] G. Orosz, *Decomposing the dynamics of delayed Hodgkin-Huxley neurons*, in Delay Systems: From Theory to Numerics and Applications, Adv. Delays Dynam. 1, T. Vyhlýdal, J.-F. Lafay, and R. Sipahi, eds., Springer, New York, 2013, pp. 343–357.
[40] G. Orosz, P. Ashwin, and S. Townley, *Learning of spatio-temporal codes in a coupled oscillator system*, IEEE Trans. Neural Networks, 20 (2009), pp. 1135–1147.
[41] G. Orosz, J. Moehlis, and P. Ashwin, *Designing the dynamics of globally coupled oscillators*, Progr. Theoret. Phys., 122 (2009), pp. 611–630.
[42] G. Orosz, J. Moehlis, and R. M. Murray, *Controlling biological networks by time-delayed signals*, Philos. Trans. Roy. Soc. Lond. Ser. A Math. Phys. Eng. Sci., 368 (2010), pp. 439–454.
[43] G. Orosz and G. Stépán, *Subcritical Hopf bifurcations in a car-following model with reaction-time delay*, Proc. R. Soc. Lond. Ser. A Math. Phys. Eng. Sci., 462 (2006), pp. 2643–2670.
[44] G. Orosz, R. E. Wilson, and G. Stépán, *Traffic jams: Dynamics and control*, Philos. Trans. R. Soc. Lond. Ser. A Math. Phys. Eng. Sci., 368 (2010), pp. 4455–4479.
[45] L. M. Pecora and T. L. Carroll, *Master stability functions for synchronized coupled systems*, Phys. Rev. Lett., 80 (1998), pp. 2109–2012.
[46] A. Pogromsky, G. Santoboni, and H. Nijmeijer, *Partial synchronization: From symmetry towards stability*, Phys. D, 172 (2002), pp. 65–87.
[47] D. Roose and R. Szalai, *Continuation and bifurcation analysis of delay differential equations*, in Numerical Continuation Methods for Dynamical Systems, Understanding Complex Systems, B. Krauskopf, H. M. Osinga, and J. Galan-Vioque, eds., Springer, New York, 2007, pp. 359–399.
[48] Y. Song, V. A. Makarov, and M. G. Velarde, *Stability switches, oscillatory multistability, and spatio-temporal patterns of nonlinear oscillations in recurrently delay coupled neural networks*, Biol. Cybernet., 101 (2009), pp. 147–167.
[49] F. Sorrentino and E. Ott, *Network synchronization of groups*, Phys. Rev. E, 76 (2007), 056114.
[50] G. Stépán, *Retarded Dynamical Systems: Stability and Characteristic Functions*, Pitman Res. Notes Math. 210, Longman, Harlow, UK, 1989.
[51] E. Steur, T. Oguchi, C. C. van Leeuwen, and H. Nijmeijer, *Partial synchronization in diffusively time-delay coupled oscillator networks*, Chaos, 22 (2012), 043144.
[52] J. Stricker, S. Cookson, M. R. Bennett, W. H. Mather, L. S. Tsimring, and J. Hasty, *A fast, robust and tunable synthetic gene oscillator*, Nature, 456 (2008), pp. 516–519.
[53] R. Szalai and G. Orosz, *Decomposing the dynamics of heterogeneous delayed networks with applications to connected vehicle systems*, Phys. Rev. E, 88 (2013), 040902(R).
[54] S. Yanchuk, P. Perlikowski, O. V. Popovych, and P. A. Tass, *Variability of spatio-temporal patterns in non-homogeneous rings of spiking neurons*, Chaos, 21 (2011), 047511.
[55] S. Yi, P. W. Nelson, and A. G. Ulsoy, *Time Delay Systems: Analysis and Control Using the Lambert W Function*, World Scientific, Singapore, 2010.